NASA Contractor Report 202322

Composite Matrix Regenerator for Stirling Engines

Timothy R. Knowles
Energy Science Laboratories, Inc.
San Diego, California

January 1997

Prepared for
Lewis Research Center
Under Contract NAS3–26249

National Aeronautics and
Space Administration

Subject: **Final Report**

COMPOSITE MATRIX REGENERATOR FOR STIRLING ENGINES

Contract: NAS3-26249 (Phase 2 SBIR)

Period covered: April, 1991 - October, 1993

Prepared by: **Energy Science Laboratories, Inc.**
6888 Nancy Ridge Drive
San Diego, CA 92121
TEL: (619) 552-2032 FAX: (619) 587-7092

Prepared for: NASA Lewis Research Center
Cleveland, Ohio 44135

Signed:

Timothy R. Knowles, Principal Investigator

Date: December 1, 1994

CONTENTS

Figures

Tables

Nomenclature

Abbreviations

CMR	composite matrix regenerator
CVD	chemical vapor deposition
CVI	chemical vapor infiltration
FEA	finite element analysis
SBR	single blow rig
SEM	scanning electron microscope
SPRE	Space Power Research Engine

Symbols

A_s	solid cross-section area for heat conduction (m^2)
c	specific heat at constant pressure (J/kg-K)
D_h	hydraulic diameter (m)
f	Fanning friction factor
G	gas mass flow rate (kg/s)
h_c	heat transfer coefficient (W/m^2-K)
j	Colburn j-factor
k	solid thermal conductivity (W/m-K)
NTU	number of heat transfer units = 4 *St* L/D_h
Nu	Nusselt number
Pr	Prandtl number
Re	Reynolds number
St	Stanton number
T	temperature (K)
t	time (s)
x	distance along sample (m)
z	dimensionless length variable = N_{TU} * x/L
α	j/f ratio
λ	kA_s / Gc_gL = conduction parameter
ρ	density (kg/m^3)
τ	dimensionless time

Acknowledgements

This work was performed under a Small Business Innovation Research (Phase 2) contract with the NASA Lewis Research Center. ESLI staff participating in this project were: John C. Oldson, N. Thomas Prokey, Juergen H. Mueller, and Timothy R. Knowles (PI).

1 PROJECT SUMMARY

The concept - This project has investigated the concept of using carbon fibers in Stirling regenerator design. The high temperature capability, strength and thermal conductivity of carbon fibers can be used advantageously in regenerator design. For high performance, regenerators must be thermally effective, have low flow impedance, low conduction losses, be mechanically stable, and operate at high temperature. An opportunity offered by high thermal conductivity (high-k) carbon fibers is to access the heat capacity of insulating walls via pin fins oriented transversely to the flow and penetrating into the wall.

To achieve higher thermal efficiency, heat engines require high temperature operation. Just as with turbine engines, Stirling engines will evolve to ever higher temperature materials, where ceramic and carbon materials are prime candidates. Because the working fluid of space Stirling power converters is helium, carbon materials are free of oxidation problems and the application seems to be a very good one for carbon composites.

Work done - Various composite configurations were investigated and fabrication experience was gained with circumferential as well as radial fiber geometries. Electrostatic fiber flocking of radial carbon fibers, followed by rigidization with carbon vapor infiltration (CVI) proved to be the best fabrication method developed in this effort. It is well suited to simple cylindrical regenerators such as used in the HP-1000 engine, and prototypes were developed for this engine. Other composite designs and geometries were investigated. Enhanced capacity regenerators in which high-k carbon fibers are used as fins to transport heat to the walls were investigated. Attempts to fabricate such composites are described highlighting the difficulties encountered. Such designs might be useful in future carbon composite regenerator development.

Analysis was performed on composite and pin fin regenerator design. The results indicate that pressure drop and heat transfer results are likely to exceed random matrix designs but not reach that of parallel plate design. In practice, cost and fabricability are drivers, and flocked carbon regenerators appear to be affordable and scalable. Axial conduction losses are intrinsically low in radial fiber geometry. Enhanced capacity wall designs may be more useful in extreme cryogenic applications (below 10 K) where heat capacity shortcomings dominate regenerator performance.

Regenerator testing was performed both in materials test rigs and in a small Ross D-60 Stirling engine. The heat transfer test rig is an innovative design, based on pulsed heating of a constant gas flow (no switching between hot and cold flows). It gives test data that can be well fitted to a simple gas heat transfer model to permit extraction of Stanton number. Pressure drops were measured in a steady-state blow rig that allowed determination of the friction factor. Engine testing showed that endurance is an issue but the CVI method eliminated the debris and permitted 10 minute endurance runs in the Ross D-60 without sign of degradation or debris, even though the engine used was noisy and vibrated strongly.

2 INTRODUCTION

2.1 Stirling Engine Regenerators

Stirling engines are of interest for meeting the growing need for space electric power and NASA has conducted several projects in Stirling technology development [Slaby, 1989]. Efforts are also underway to develop Stirling engines for terrestrial solar power and automotive transportation [Simetkosky, 1986]. Stirling heat pumps and cryocoolers are related machines that are being actively developed by both Government and industry.

The Stirling engine is an external combustion heat engine based on an ideal thermal cycle as efficient as the Carnot cycle. Actual Stirling engines do have comparatively high efficiency, typically between 20% and 60% of the theoretically maximum Carnot efficiency. External combustion also permits the use of various heat sources, including nuclear and solar energy, as well as fossil and other chemical fuels. The steady external combustion process permits Stirling engines to utilize fossil fuels while creating less pollution than internal combustion engines. However, the steady high temperatures entail materials problems that have prevented Stirling engines from gaining wide acceptance.

The Stirling engine contains an internal heat exchanger component, the regenerator, which is sometimes referred to as the "heart" of the Stirling engine, because it is responsible for the critical temperature changes in the working fluid during the constant volume processes that characterize the Stirling cycle. A typical engine regenerator may be steel wool packed into an annulus having a 10 cm inside diameter and a square cross-section 1 cm wide. Its effectiveness sensitively influences the overall engine efficiency. Problems associated with making effective regenerators stem from limitations of the traditional materials used. They are subjected to extreme conditions of hot oscillating gas flow and high temperature gradients. For high performance, regenerators should be thermally insulating in the (axial) direction of the temperature gradient and should exchange heat rapidly with the working fluid. They should have minimum dead volume in the regenerator, as dead volume reduces the engine compression ratio. The flow of gas through the regenerator matrix introduces drag and viscous losses, which one would like to reduce. Efforts at reducing some of these loss mechanisms tend to aggravate others.

Prototype Space Stirling Engines currently use random metal matrix regenerators. The individual steel filaments of the Brunswick felt material are typically 25 μm in diameter and several millimeters in length. The arrangement of the steel filaments, aligned primarily perpendicular to the flow direction and touching each other only at points, mitigates the potentially large conduction losses of such metallic filaments. In order that the metal interact well thermally with the gas, it must be dispersed as such fine filaments, and they may not be spaced too widely. It is a goal of regenerator design to reduce the net loss associated with these mechanisms. Composite regenerator design offers new possibilities in terms of high temperature materials and flow channel architecture.

2.2 Composite Matrix Regenerator Concept

Thermal composite materials are composites of high-k and high-c materials tailored for specific thermal applications [Knowles, 1987]. The purpose in compositing is to combine materials that individually have certain outstanding properties to obtain new materials having desired combinations of those properties. For example, fiber-resin composites are useful structural materials possessing both high tensile strength and high compressive strength inherited from the fiber and resin components, respectively. Thermal composites are created to meet particular thermal applications, using components that each have a desired property. Compositing allows vastly more materials possibilities than available with homogeneous materials, and in particular allows materials combinations and architectures suitable for use in Stirling engine regenerators.

The thermal conductivity (k) of graphitized carbon fibers is $k \sim 300$ - $1000\ \mathrm{W\,m^{-1}\,K^{-1}}$, which is high compared to stainless steel having $k \sim 15\ \mathrm{W\,m^{-1}\,K^{-1}}$. Transverse to the fiber axis the k is roughly 100-times smaller so that, when a composite is formed with a low-k matrix, the resulting fiber composite has highly anisotropic conduction properties. For regenerator applications, such fibers can be used effectively to extract heat from the gas flow and conduct it into a high-c, low-k channel wall. The resulting regenerator is referred to here as a composite matrix regenerator (CMR). For engine applications the potential benefits of CMRs are:

- parallel duct flow channels having higher effectiveness for a given flow friction than either packed spheres, felts or stacked screens
- gas/solid heat transfer enhancement resulting from high fiber surface area in the flow channels between the plates, enabling the use of fewer, larger flow channels that are potentially more easily fabricated
- uniform pressure drop across the flow channels caused by fibers in cross-flow (a reduction of the flow maldistribution effects common in parallel plate regenerators)
- lower pressure drop and lower dead volume than for conventional regenerators

A basic configuration for a fiber CMR is shown in **Fig. 1** along with other common configurations. The concept is based on using high-k fibers oriented transversely to the flow direction. **Table 1** lists various possible implementations of the CMR concept.

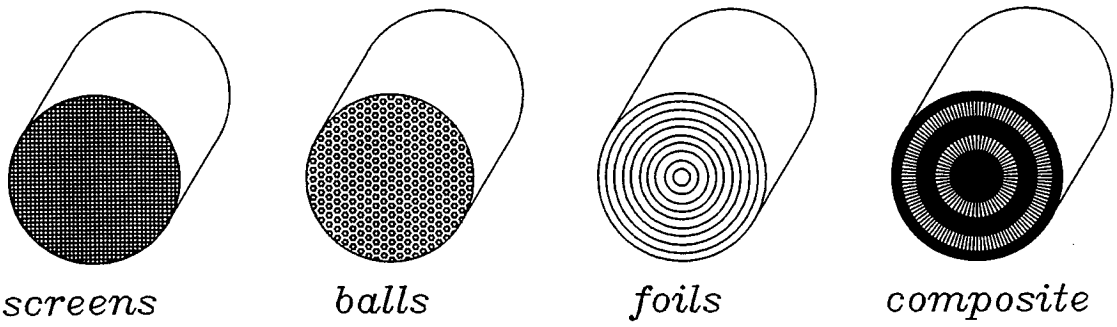

Fig. 1 The composite matrix regenerator concept compared with other regenerator types.

Table 1 CMR design configurations.

1 Component materials
- 1.1 high-k carbon fiber
  - P-120, CCVD, isotopically pure materials
  - flocked, injected fibers
- 1.2 ceramics
  - alumina film
- 1.3 high char organics
  - phenolic, pitch

2 Planar duct structures
- 2.1 Microcell structures
  - balsa
  - filter
  - avian lung
- 2.2 Scrolled metal foils
  - stainless steel foil (Fraenkel packing)
  - slotted metal foil
- 2.3 Honeycombs
  - ceramic heat exchanger/recuperator
  - paper honeycombs
- 2.4 Slotted carbon-carbon annulus

3 Crossflow structures
- 3.1 screens/meshes/gauzes
- 3.2 stainless steel felt (Brunswick/Technetics)
- 3.3 metex braid
- 3.4 carbon felts
- 3.5 carbon flocks

4 Hybrid, fiber channel structures
- 4.1 flocked honeycomb
- 4.2 channeled filament tape
- 4.3 fiber platelet laminations

Issues - The fabrication difficulty in implementing CMRs is the uniform placement of fibers transverse to the flow and in good thermal contact with the matrix material. The matrix material that defines the flow channel boundaries must also be tough enough to withstand the engine environment without generating debris.

2.3 Project Objectives

This Phase 2 SBIR project concerns the fabrication development and initial testing of fiber CMRs for use in space Stirling engines. CMRs are made of thermal composite materials that incorporate separate conductivity and capacity components tailored for potentially higher regenerator thermal effectiveness and lower viscous loss than achieved with conventional felt, metal screens and scrolls, or extruded ceramic regenerators. Composite materials processing potentially enables cost-effective fabrication of microchannel structures having anisotropic heat transfer properties. If successful, the benefit to NASA is higher performance, lower cost space power. Spin-offs are anticipated for regenerators of terrestrial Stirling engines, heat pumps and coolers, as well as general high performance heat transfer materials and equipment.

Desired properties of a Stirling engine regenerator are: good thermal effectiveness, low pressure drop, low dead volume, low axial conduction loss, compatibility with the engine environment and acceptable wear . Existing regenerators have one or more weakness on the basis of this list. For example: scrolled steel has high conduction loss, steel felt or screen has high viscous loss, and extruded ceramic has low thermal effectiveness. Conceptually more effective designs based on platelet technology or etched foils are currently expensive and will not meet the high temperature requirements of future space engines.

Phase 2 development effort addressed the processing of composite planar duct structures having low axial conduction and good thermal effectiveness. Of particular interest are hybrid structures in which the crossflow graphite fibers allow the use of wider channels and thicker walls that offer lower pressure drop, while maintaining high thermal effectiveness. The technical objectives are to develop fabrication techniques, obtain data on CMR properties, develop modified Stirling cycle analysis code accounting for CMR behavior, obtain engine performance data, and fabricate a Prototype CMR deliverable for a NASA Stirling engine application such as space power converters. The project tasks are listed below.

Task 1 **DEVELOP CMR FABRICATION METHODS.**
Task 2 **DEVELOP THERMAL/FLUID-DYNAMIC MODELING.**
Task 3 **MEASURE CMR PROPERTIES.**
Task 4 **ENGINE TEST CMR PERFORMANCE.**
Task 5 **DESIGN & FABRICATE PROTOTYPE CMR FOR NASA STIRLING ENGINE.**
Task 6 **REPORTING.**

3 COMPOSITE MATRIX REGENERATOR DEVELOPMENT

For the prototype CMR, this project initially targeted the 12.5 kWe output NASA Space Power Research Engine (SPRE), whose regenerators are large. The target shifted to the 1-kWe HP-1000 engine whose regenerators are smaller. This engine was determined to be a more suitable test bed.

3.1 CMR Fabrication Trials

Several candidate fabrication methods were investigated including machining of carbon-carbon, the scrolling of carbonizable foils and fiber tapes into annular regenerator structures, and electrostatic fiber positioning for crossflow regenerator structures. The various attempts and lessons learned are summarized. The fabrication method used for producing Prototype regenerators for the HP-1000 Stirling engine is based on the electroflocking of carbon fibers (Section 3.1.3) followed by carbon vapor infiltration to increase the fiber diameter and heat capacity, and that method is described in more detail in Section 3.5

3.1.1 Machining

A carbon-carbon disk 7.5 cm in diameter and 1.7 cm thick was machined with 0.25 mm slots for illustration purposes (**Fig. 2**). Total set up and machining effort was less than 4 man-hours,

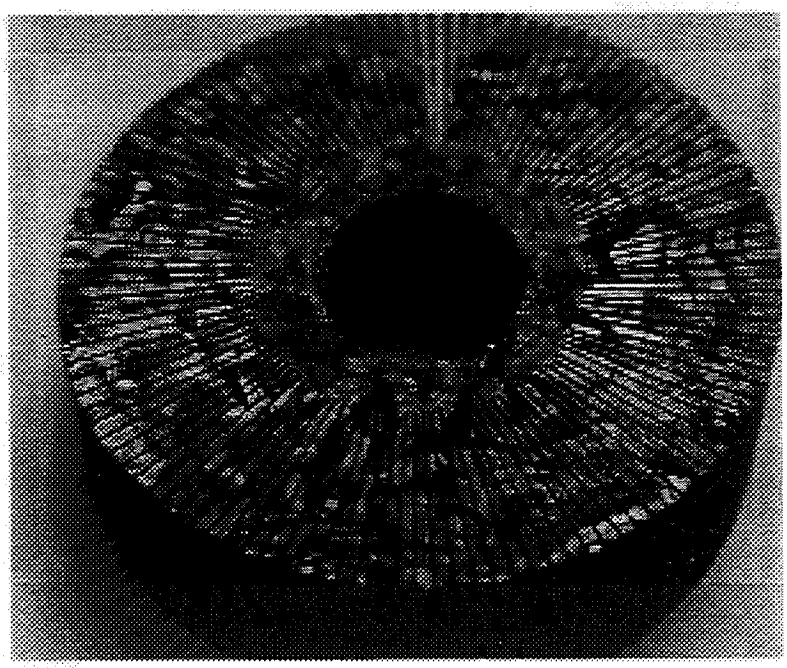

Fig. 2 Carbon-carbon disk machined with 0.25 mm thick slitting saw.

illustrating the ease of machining this material. The radial slots were cut with a 0.020" slotting saw mounted on an end mill with a vertical rotary table. The thermal effectiveness of this design is expected to be low, and better designs would require smaller slots and thinner walls, typically on the order of a few mils.

The possibility of machining finer structures was investigated. Electric discharge machining is slow and therefore expensive on carbon. The possibility of slotting carbon-carbon with an array of hot wires in an oxidizing environment was evaluated. Attempts at machining into pyrolytic graphite with a single hot wire were fruitless, although it proved easy to cut through common charcoal. The carbon microstructure in these materials is very different. The porous amorphous carbon of the charcoal is easily removed, but the dense graphite of the pyrolytic carbon is far less reactive to heating in air. Similar results were observed with an oxidizing microtorch and these machining techniques were not pursued further.

3.1.2 Scrolling

Machining small slots into carbon-carbon for regenerator applications is prohibitively expensive. As an alternative to machining, foils can be incorporated in the precursor matrix to be extracted after the part has set. **Fig. 3** shows successful results with a 1 mm thick soft solder film that was potted in phenolic prior to processing. To be useful, slots with thickness ~0.1 mm are

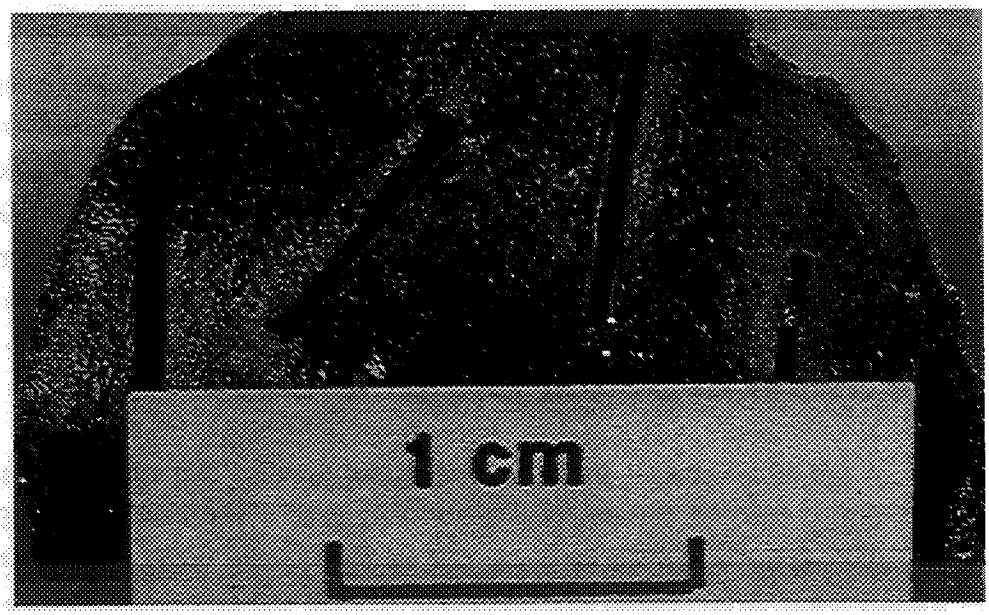

Fig. 3 Slots in a carbon part produced using soft solder foil (1 mm thick) in a graphite loaded phenolic matrix. The solder was melted away after cure and prior to carbonization.

required at a spacing of ~0.1 mm. Attempts to chemically etch the aluminum foil out of the composite were unsatisfactory, because an insoluble residue formed that inhibited dissolution.

Slotted Foil - Electrolytically patterned foil was obtained for use in testing scrolled regenerators. Stork Veco International supplied 316 stainless steel, 4 mils thick, with slots 5 mils wide and 52 mils long, and 21% open area. Although the pattern is not ideally suited for the purpose of low thermal conductivity, it may be substantially better than an ordinary 316 stainless steel scrolled regenerator for suitable, lower frequency engine speeds. This material is a candidate for testing in the Ross D-60 Engine. Note that MTI reported good results in the 1990 IECEC Proceedings using an ordinary scrolled foil regenerator.

Large Scrolled Regenerator - To illustrate the concept of a paper-derived regenerator, a 9-inch annular roll of paper admission tickets was corrugated and impregnated with phenolic resin. The paper thickness was 0.014" and an in-house corrugator consisting of a pair of metal gears produced a corrugation amplitude of 0.037". A bilayer consisting of one corrugated strip and one non-corrugated strip were rolled together producing an annular structure 5.3" ID × 8.8" OD. The initial paper mass was 203 g. This scrolled structure was impregnated with a solution consisting of 5 volume parts methanol + 4 volume parts Stuart-Ironsides DP25-10 Phenolic Resin. The solution was poured over the paper, allowed to drain, and then compressed air was blown through the passages in the scroll to clear them. The phenolic-impregnated paper scroll was then cured at 105°C for 1 hr. The impregnation and cure was repeated a total of three times to increase density and provide greater strength. A layer of undiluted phenolic was applied to the ID and OD to provide more strength there. The phenolic impregnation increased the mass of the scroll to 403 g.

The scroll was then carbonized to 750°C in a closed stainless steel chamber with a flowing nitrogen atmosphere in an oven. A thermocouple in the chamber was used to monitor temperature. At approx. 400°C voluminous outgassing occurred. After two hours 750°C was reached and held for 2 hr. The power was then switched off and the sample allowed to cool at approx. 100°C/hr.

Fig. 4 shows the appearance after carbonization. The scroll became brittle and flaky, but could be handled. The original 1" thickness changed to 0.84" and the OD changed to approx. 7". The final mass was 168 g, only 42% of the mass prior to carbonization. These results were considered justification to consider further this approach to carbon regenerator processing. Required is the development of stronger and finer-celled regenerators with adequate net shape precision.

Grafoil - A foil of compressed grafoil was corrugated, scrolled into a tight coil and stabilized with a phenolic wash. It was observed to give very good dimensional stability (**Fig. 5**, **Fig. 6**), but it is rather expensive and has excessive thermal conductivity in the axial direction. For comparison purposes a low density paper was corrugated, scrolled and impregnated with phenolic resin. The corrugation distorted strongly during carbonization. Further attempts using resins with carbon black as additives gave similar results. **Table 2** lists the mass changes during processing of the various paper samples investigated.

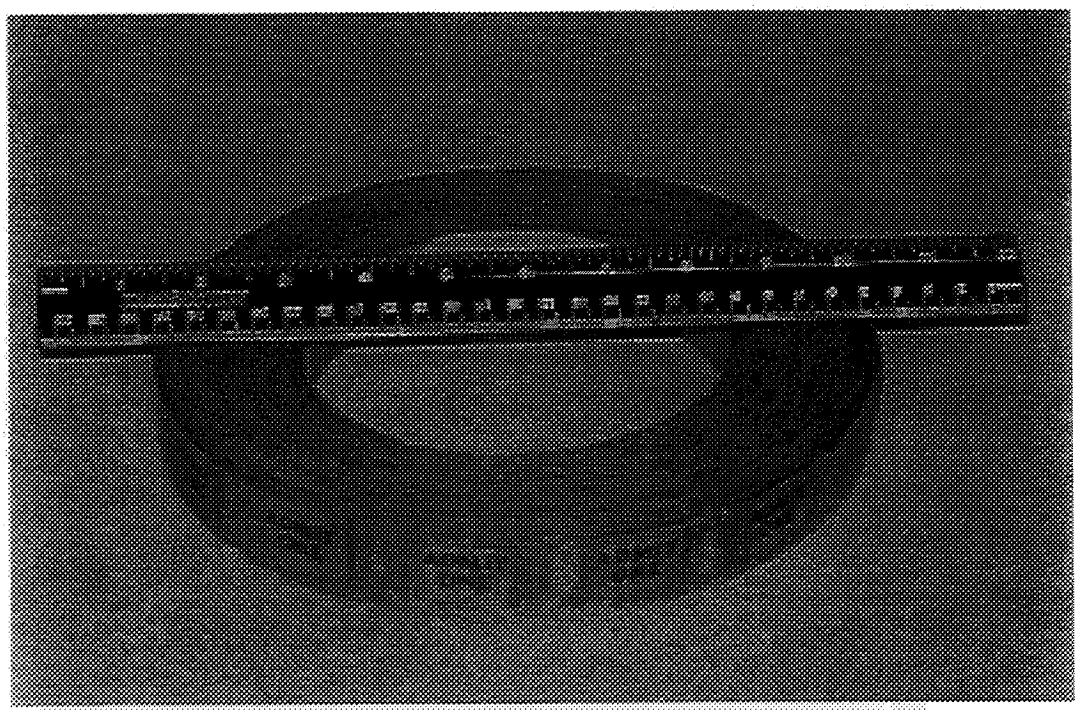

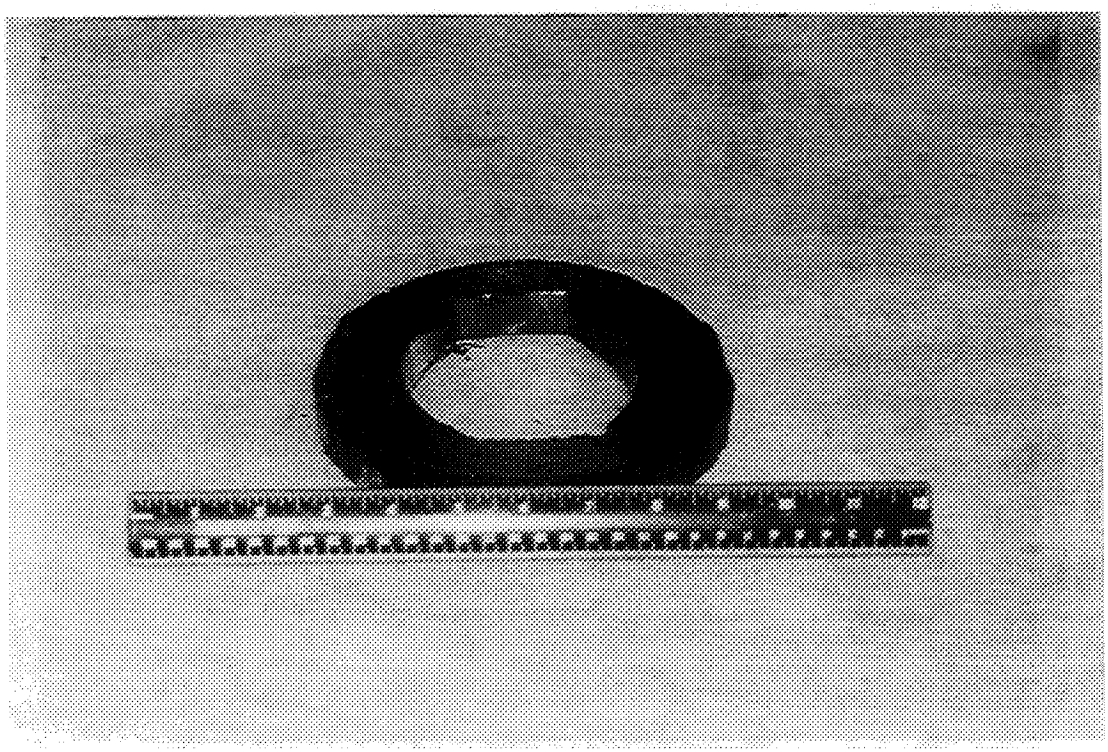

Fig. 4 Scrolled Regenerator No. 01 before and after carbonization.

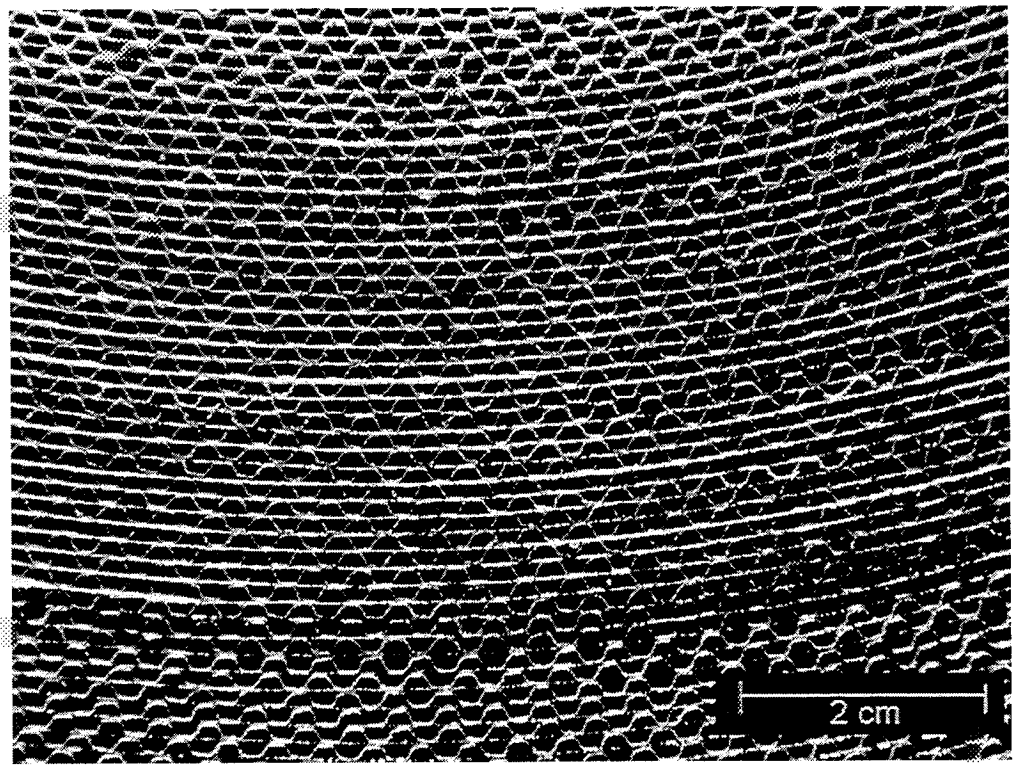

Fig. 5 Corrugated Grafoil scroll, stabilized with phenolic and carbonized.

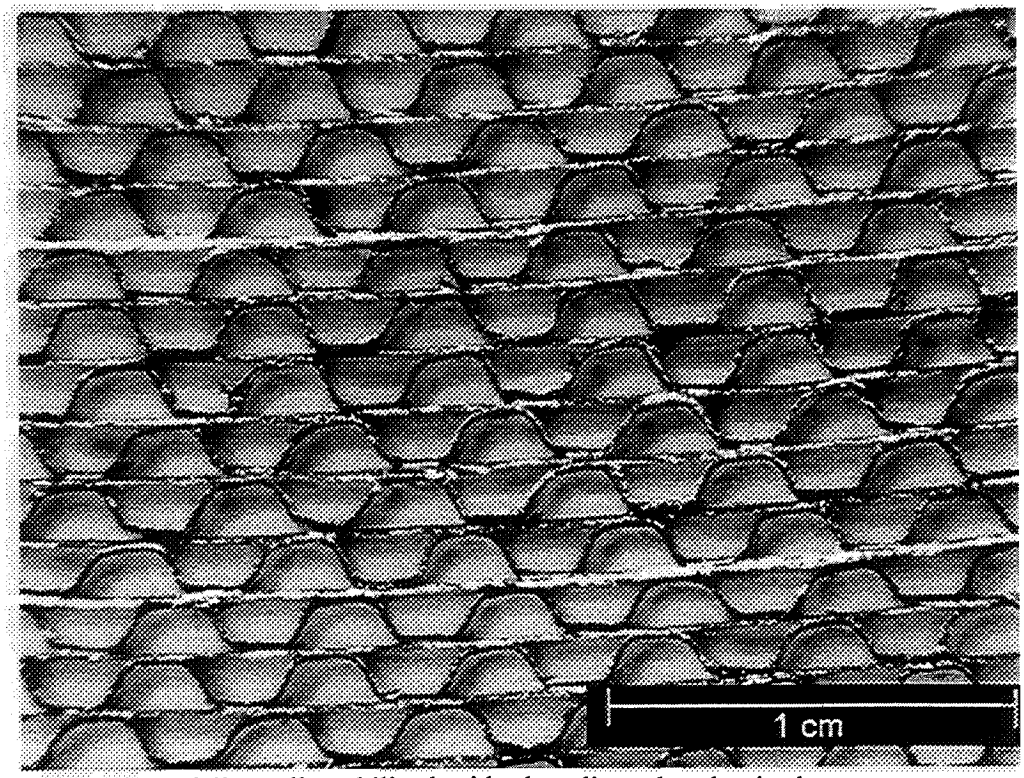

Fig. 6 Corrugated Grafoil scroll, stabilized with phenolic and carbonized.

Table 2 Mass changes during processing of scrolled regenerator samples.

MATERIAL TYPE	MASS (g)			SIZE (in)		
	Initial	Final	% Loss	Initial	Final	% shrink
ceramic paper, phenolic coated	24.47	13.94	43.0%	1.8	1.65	8.3%
ceramic paper, phenolic and carbon coated	21.23	12.79	39.8%	1.65	1.45	12.1%
rayon cloth, phenolic coated	2.64	1.11	58.0%	1	0.95	5.0%
scrolled newsprint, super - glue, phenolic coated	2.02	0.5	75.2%	0.6	0.45	25.0%
cotton paper, phenolic coated	3.25	0.8	75.4%	1.1	1	9.1%
computer paper, phenolic coated	5.48	2.62	52.2%	1	1.1	10.0% (expansion)
computer paper, phenolic and carbon coated	5.49	2.68	51.2%	1.35	1.25	7.4%
rolled carbon felt	0.93	0.39	58.1%	1.05	1.05	0.0%
porous phenolic plug	1.44	0.77	46.5%	1	0.8	20.0%

Polyimide matrix - Polyimide-film/carbon-fiber composites were investigated. Kapton film, a commercial polyimide, was printed with a transverse slot pattern and layered with carbon fibers. The composite was then pyrolyzed by heating to 800°C over approximately 3 hrs. The appearance of the sample before and after processing is shown in **Fig. 7**. The pronounced shrinkage of the film relative to the fibers has caused breakage of some fibers. The curling of the film can be prevented quite easily by clamping the film between carbon plates during pyrolysis, but it is apparent that the shrinkage of the thermoset films does not permit the winding of a patterned kapton film with fiber reinforcement.

For use with continuous carbon fiber, it is critical to identify a matrix material that can be used in conjunction with carbon fibers that do not shrink at all during thermal processing. Since resin matrices generally shrink by up to 25%, it is difficult to laminate or layer thermoset films with carbon fibers that do not shrink. More likely is to apply the resin directly to the fibers with the intention that the matrix will shrink toward the fibers during cure and pyrolysis of thin uniaxial fiber hoops. To test this idea, polyamic acid (the polyimide precursor) was applied directly to the carbon fibers and these coated fibers were processed. **Fig. 8** shows the successful result that the coated

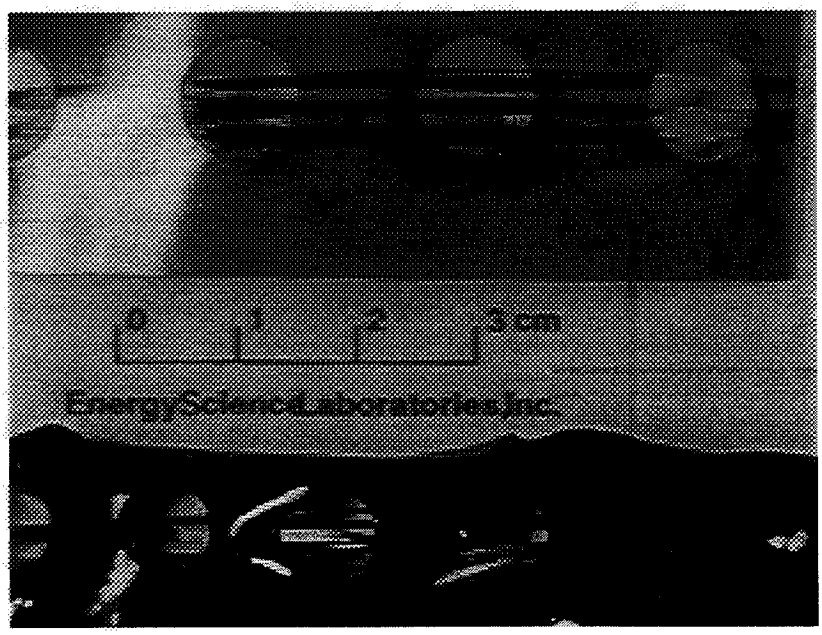

Fig. 7 Carbon fibers layered with kapton film, before (top) and after (bottom) pyrolysis treatment, showing how the film shrinks away from the fibers.

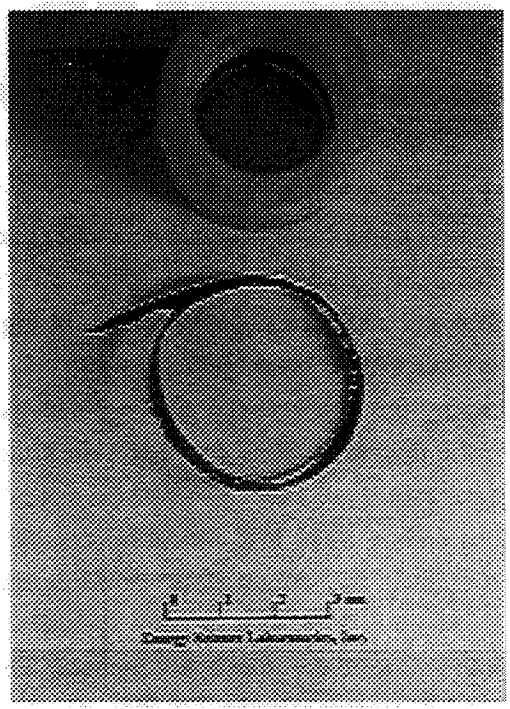

Fig. 8 Ring of carbon fibers potted in polyimide resin, cured and pyrolyzed together, showing no shrinkage in the radial direction. The matrix shrinks toward — not away — from the fibers during processing, which is desired.

fibers are not deformed or broken by shrinkage of the matrix. Noticeable shrinkage occurs along the axial direction, consistent with the shrinkage of the matrix *toward* the fiber, but not away from it in the radial direction, as was the case with the kapton film experiment shown in Fig. 7. This result encourages us to pursue a design in which the precursor is applied to a monolayer tape of carbon fibers. The resulting coated tape could be wound onto a mandrel and processed to high temperature to produce a carbon-carbon regenerator structure.

Ceramic Tape - Ceramic films are candidate matrix materials with useful thermal properties (**Table 3**) for use in conjunction with carbon fibers in a regenerator matrix. The concept is to print ceramic slurries onto thin fiber tapes, that may then be wound or stacked. Fine cordierite powder (magnesia alumina silica) was obtained from Mussel Shoals Mineral Company (FL) and lithium alumina silica (LAS) powder from Corning Glass (NY). Both of these ceramic materials have a low coefficient of thermal expansion and high thermal shock resistance, making them candidates for high temperature regenerator and heat exchanger applications. Tape casting was performed using the following components:

Solvents:	Toluene or Trichloroethylene and Ethanol
Dispersant:	Menhaden Fish Oil
Binder:	Polyvinyl Butyral
Plasticizer:	Polyethylene Glycol, Octyl Phthalate

Means of printing ceramic matrix onto tows of dispersed carbon fibers were briefly investigated. The first material used was a fine cordierite powder (magnesia alumina silica) that adhered to the fiber throughout cure at 200°C and sintering at 900°C. Fiber pre-coating with an aqueous suspension of graphite flake (AquaDag from Acheson Carbon) further improved adhesion. Unlike the strong wicking behavior observed with carbonaceous resins, the wet ceramics do not wick but do adhere well. We observed that the fired cordierite film was weak and the supplier confirmed that we had used a fine powder with a narrow distribution of particle size. Stronger materials are possible with a range of particle sizes.

The printed powder produced 0.010" thick films. The powder coarseness prevented the ceramic from printing through a dense unidirectional carbon fiber tape 0.010" thick and resulted in a 0.010" thick layer printed on top of the fiber tape. A finer grain cordierite is required either from a supplier or by ball milling our current supply. **Fig. 9** shows SEM photos of carbon fiber samples coated with different precursors to illustrate the wetting and porosity as processed.

Masks were used to permit patterning of the stripes defining the flow channels. Two requirements of an acceptable mask are: 1) permit processing at T > 100°C; and 2) resist ketone solvents present in the phenolic resin. The two most successful candidates were methyl cellulose (Methocel) and latex. These materials were applied to a thin carbon paper by scraping through a 0.001" thick stencil patterned with parallel stripes 0.1" wide, separated by 0.1". The Methocel is applied as a hydrated gel and is then dehydrated in an oven at 100°C, forming a 0.001" dry film

Table 3 Materials properties of selected regenerator materials (T = 750 K).

Material	k (W/K-cm)	d (g/cm^3)	c_p (J/g-K)	c (J/cm^3-K)	kc	k/c	kc (normalized to steel)	k/c (normalized to steel)
Stainless Steel	0.14	8.00	0.66	5.28	0.74	0.027	1.00	1.00
Graphite (crystal)	5.20	2.10	1.81	3.80	19.77	1.368	26.74	51.60
Carbon (amorphous)	0.02	2.10	1.81	3.80	0.09	0.006	0.12	0.24
Silicon	0.30	2.33	0.94	2.19	0.66	0.137	0.89	5.16
Boron	0.06	2.34	2.32	5.44	0.34	0.011	0.46	0.43
Beryllium	0.87	1.85	3.05	5.64	4.90	0.154	6.63	5.80
50%Graphite/Carbon	2.61	2.10	1.81	3.80	9.93	0.687	13.43	25.92
50%Graphite/Boron	2.63	2.22	2.08	4.62	12.15	0.570	16.44	21.48
50%Graphite/Silicon	2.75	2.22	1.35	3.00	8.24	0.918	11.15	34.61

which can be removed by mild oxidation that does not affect the carbon fibers. The latex films applied were 0.003" thick. It appears that the latex becomes more difficult to dissolve away after heat treatment at 100°C, and is therefore the less successful of the two candidates investigated. The processing approach attempted is: (1) Start with a continuous 1" wide tape of longitudinal carbon fibers, approximately 2000 fibers spread over 1" (less than one monolayer coverage); (2) Apply a continuous pattern of 1-mil thick transverse ceramic stripes across the 1" width of the tape as the tape is transferred from a supply reel to a take up reel. The stripes are roughly 0.05" wide and have a 0.10" pitch; (3) Reel up the tape forming the regenerator requiring only final machining to net shape. This approach produces a "filament tape" structure with involute flow channels 0.05" wide and involute walls 0.05" wide. The flow direction is axial.

Cordierite ceramic tape - A continuous cordierite film 0.002" thick, 2" wide and approximately 100' long was acquired from Wallace Technical Ceramics (San Diego). Strips of film were cut and then alternating layers of continuous and slotted films were stacked to create flow passages 0.185" x 0.002". This layered ceramic structure was fired at a rate of 250°C/hr to 1000°C with 500 psi compression force. The resultant piece showed no deformation but was powdery and seemed to be incompletely fired. The firing was repeated without the compressing weights to a higher temperature of 1100°C. The result was then a quite deformed structure with poor definition of the flow passages. Interlaminar bonding was also poor, and the edges of the structure crumbled quite easily just under rubbing. This approach did not succeed in integrating carbon fiber tows with this sort of tape.

(a)

(b)

(c)

Fig. 9 SEM photos of carbon fibers in (a) cordierite, (b) polyimide, and (c) saran precursors.

Scrolled unidirectional carbon fiber prepreg - The next concept investigated was scrolling a carbon fiber prepreg with a spacing film of a low melting paraffin wax. A 0.005" thick paraffin film (Parafilm) was attached to a 0.010" thick unidirectional carbon fiber tape (Orcoweb G-450, 1.74 g/cm^3). The fiber tape was impregnated with a thin phenolic resin and scrolled together with the film. The scroll was then cured at 85°C for 12 hours and 100°C for 8 hours. The low cure temperatures and longer cure times were required to minimize deformation of the Parafilm during cure. The cured scroll was then carbonized at 900°C in a nitrogen atmosphere. The resulting scroll was quite weak, and generated carbon debris.

Carbon felts - Carbon felts are available from AMOCO (Ridgefield, CT), Ashland (Ashland, KY) and AFN Products (NY). These felts are available in various densities, typically 0.2 — 2.0 oz/sqyd. **Fig. 10** shows micrographs comparing the Ashland 1 oz/sqyd (2.43% density) carbon felt with the 16% density, 12.5 μm Brunswick Technetics stainless steel felt. Carbon felts may be useful in regenerator applications, because they have low axial conduction loss and are very inexpensive. Problems with using carbon felts are the comparatively low volumetric heat capacity (**Table 4**) and structural weakness, but these problems may be overcome by suitable packing and infiltration.

Striped carbon felt - For the circumferentially wound carbon fiber CMR ("fiber tape regenerator") a resin material is required that can print stripes on a tape of carbon fibers. For the precision required (1.0 mm ± 0.1 mm) the resin should not wick strongly, nor should it shrink and deform the fiber tape during thermal processing. The standard phenolic and polyimide resins investigated previously were not suitable and a colloidal graphite suspension (available from Acheson Chemicals) was investigated. This gel product is easy to work with and **Fig. 11** shows a sample of a carbon felt strip (International Paper, 6.8 g/cm^2) that has been coated with this form of carbon. The graphite paint consists of micron-scale flakes which potentially could generate debris. To increase its strength and reduce the debris potential, a lamellar graphite coating ~2 μm thick was deposited by methane chemical vapor deposition (CVD). **Fig. 12** shows micrographs of the graphite paint with and without the coating.

Table 4 Carbon and steel thermal properties.

Material	heat capacity (J/K-g)	thermal conductivity (W/K-m)	density (kg/m^3)
felt carbon	0.712	0.035	1570
316 stainless steel	0.494	16.23	9058
Inconel-600	0.456	15.00	8498

(a)

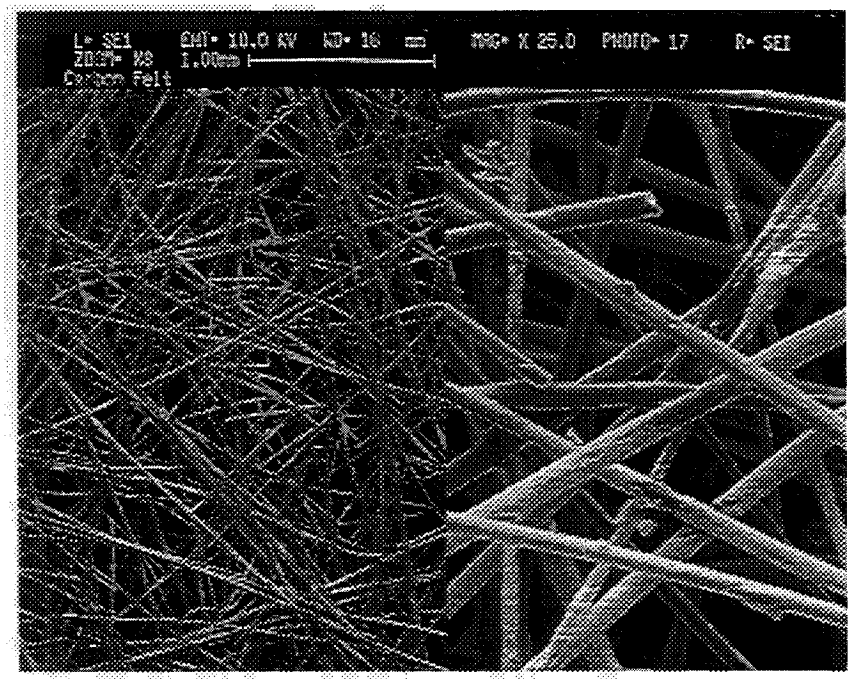

(b)

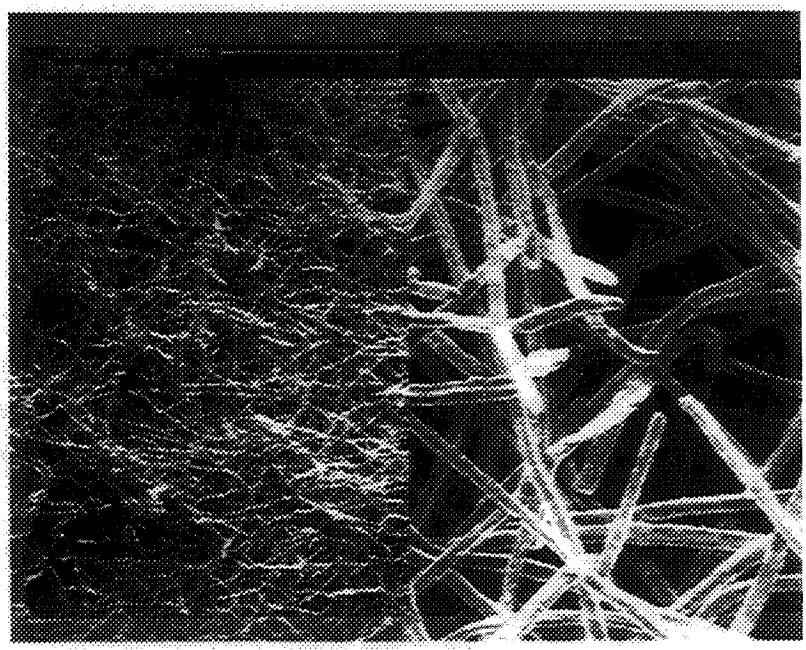

Fig. 10 SEM photos of (a) carbon and (b) steel felts.

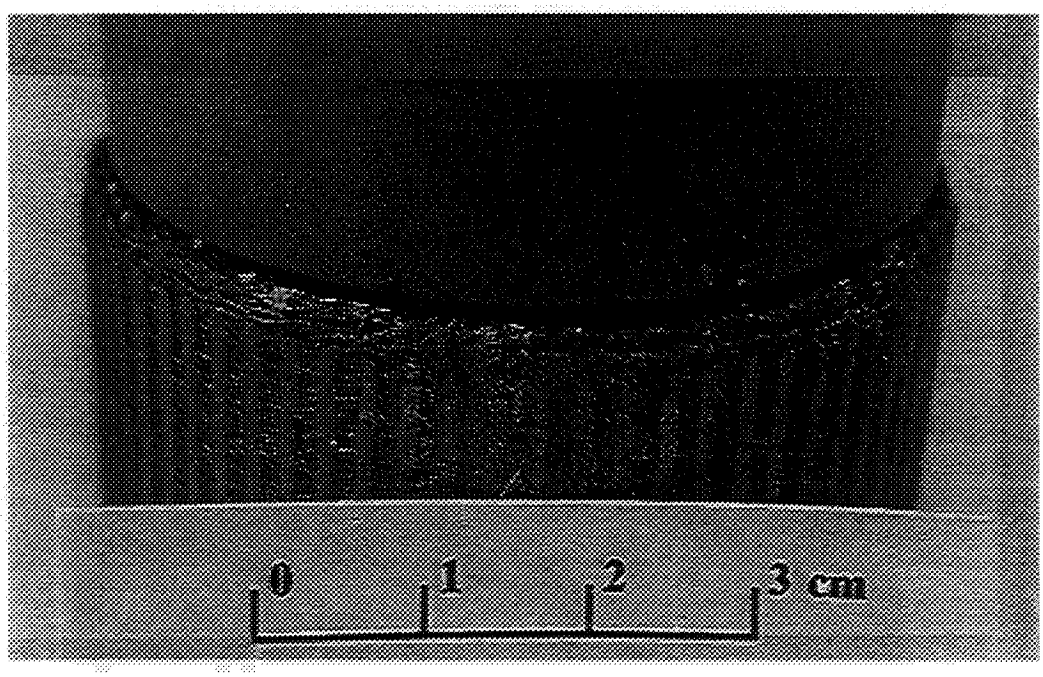

Fig. 11 Carbon felt printed with stripes of colloidal graphite paint and heated to 1000°C.

Scroll Patterns - The patterns resulting from scrolling a slotted tape were investigated to understand the flow channel pattern resulting from the winding of a slotted tape having a fixed pitch. The pattern of flow passages is simulated by drawing a multiturn spiral curve with a dashed line, such that the slot width, spacing and the pitch of the spiral correspond to the slot pattern and thickness of the tape. The drawings were generated with an HP-7550 Plotter controlled by a simple BASIC program. For a spiral whose radius satisfies

$$r = \alpha \theta$$

the arc length, s, is given by

$$s = (\alpha / 2) [\theta (1 + \theta^2)^{1/2} + \ln(\theta + (1 + \theta^2)^{1/2}]$$

The plotter was instructed to draw a spiral curve corresponding to the full scale SPRE regenerator, such that the scroll layer thickness equaled that of the proposed lay-up tape and the pen was moved up or down at the proper arc length values to produce the regular pattern of the slotted tape. The resulting patterns can be quite complicated because the successive wraps of the tape have increasing lengths and therefore increasing numbers of slots per turn. In studying numerous patterns there appeared highly "organized" patterns as well as very "disorganized" patterns. The degree of organization depends sensitively on the following dimensionless parameter:

$$\delta n = 2\pi t / p$$

where t = tape thickness and p = pitch length of slot pattern.

(a)

(b)

(c)

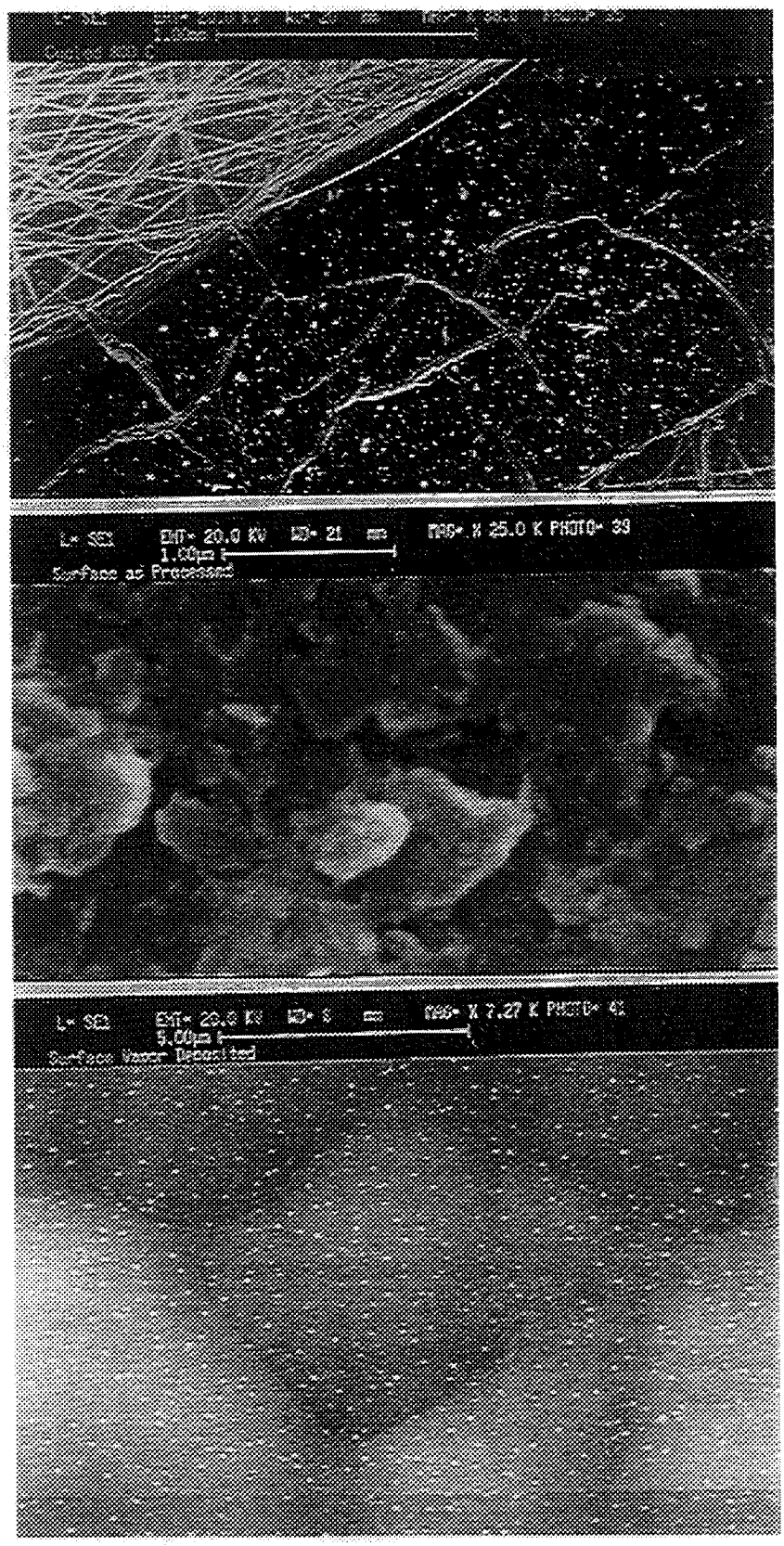

Fig. 12 (a) Carbon stripe, (b) detail of carbon stripe showing flake microstructure, (c) flake microstructure after methane CVD coating with 2 μm of lamellar graphite.

When δn is an integer or simple fraction, radial channel features arise in certain directions on the scroll, as illustrated in **Fig. 13**. When δn is slightly different than such integer values the radial features begin to lean over ("involute") and, as δn differs more, the channel pattern can show "cusp" features. It appears that the cusped patterns present a rather uniform porosity across the face of the regenerator and are therefore preferred. **Fig. 14** shows a candidate pattern for SPRE dimensions (shown here at 2/3 scale to fit on the page) at channel porosities 50% (ie. the dash length equals the gap length in the scroll pattern).

The smoothness of the crescent-shaped flow channels as a function of the tape thickness was investigated, and **Fig. 15** shows (a) the baseline case (thickness = 27 mil), (b) at half thickness, 13.5 mil and (c) at quarter thickness, 6.75 mil. Pattern (b) is magnified 2x pattern and (c) is magnified 4x for better visualization.

The scroll patterns resulting from a bilayer scroll consisting of a continuous layer and a slotted layer have been plotted as a spiral of two parallel lines, one solid and one slotted with 50% open area, making for 25% overall porosity. The results are shown in **Fig. 16** and **Fig. 17**.

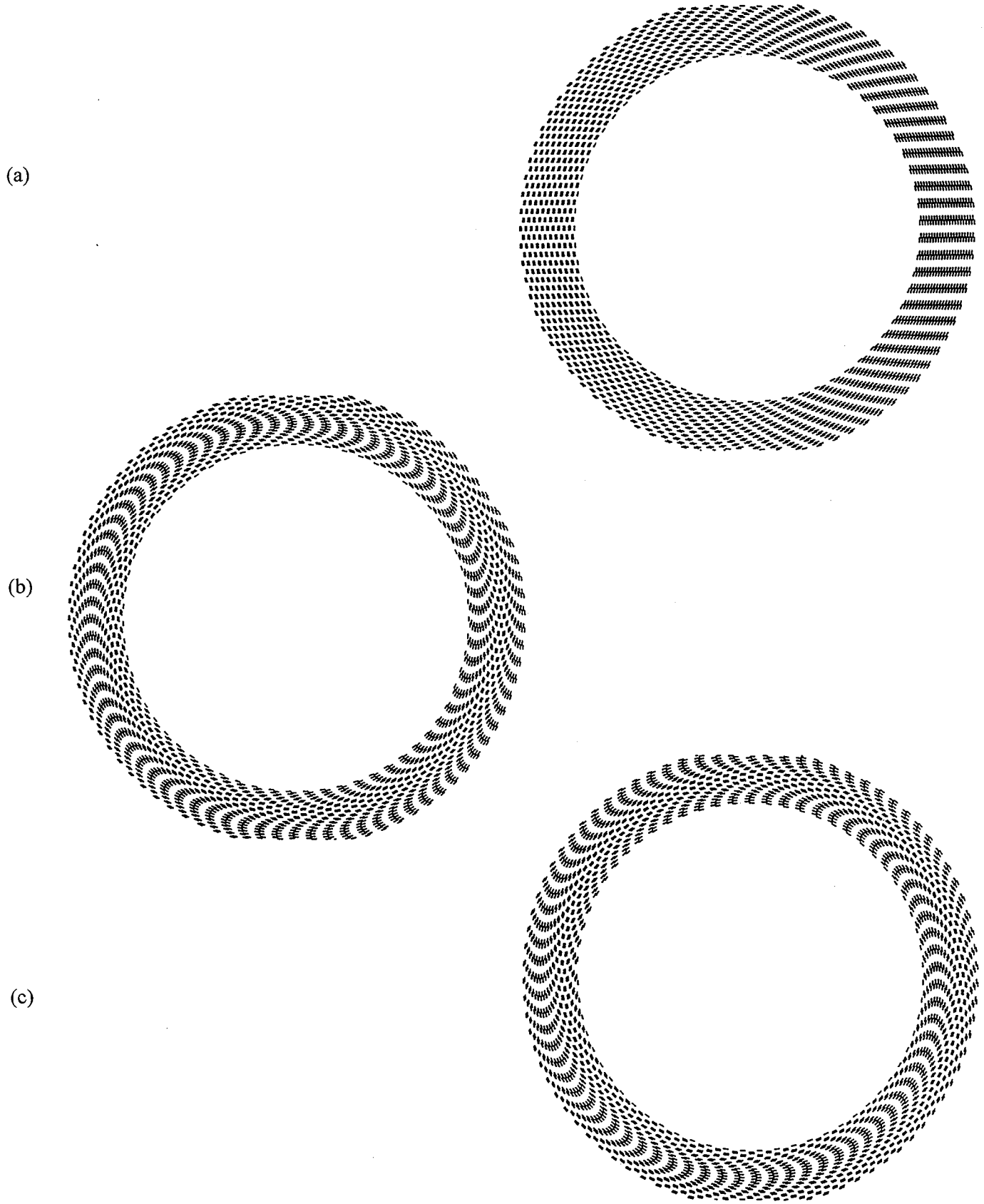

Fig. 13 Spirals created with dashed lines in which (a) $\delta n = 0.5$, (b) $\delta n = 0.49$ and (c) $\delta n = 0.51$.

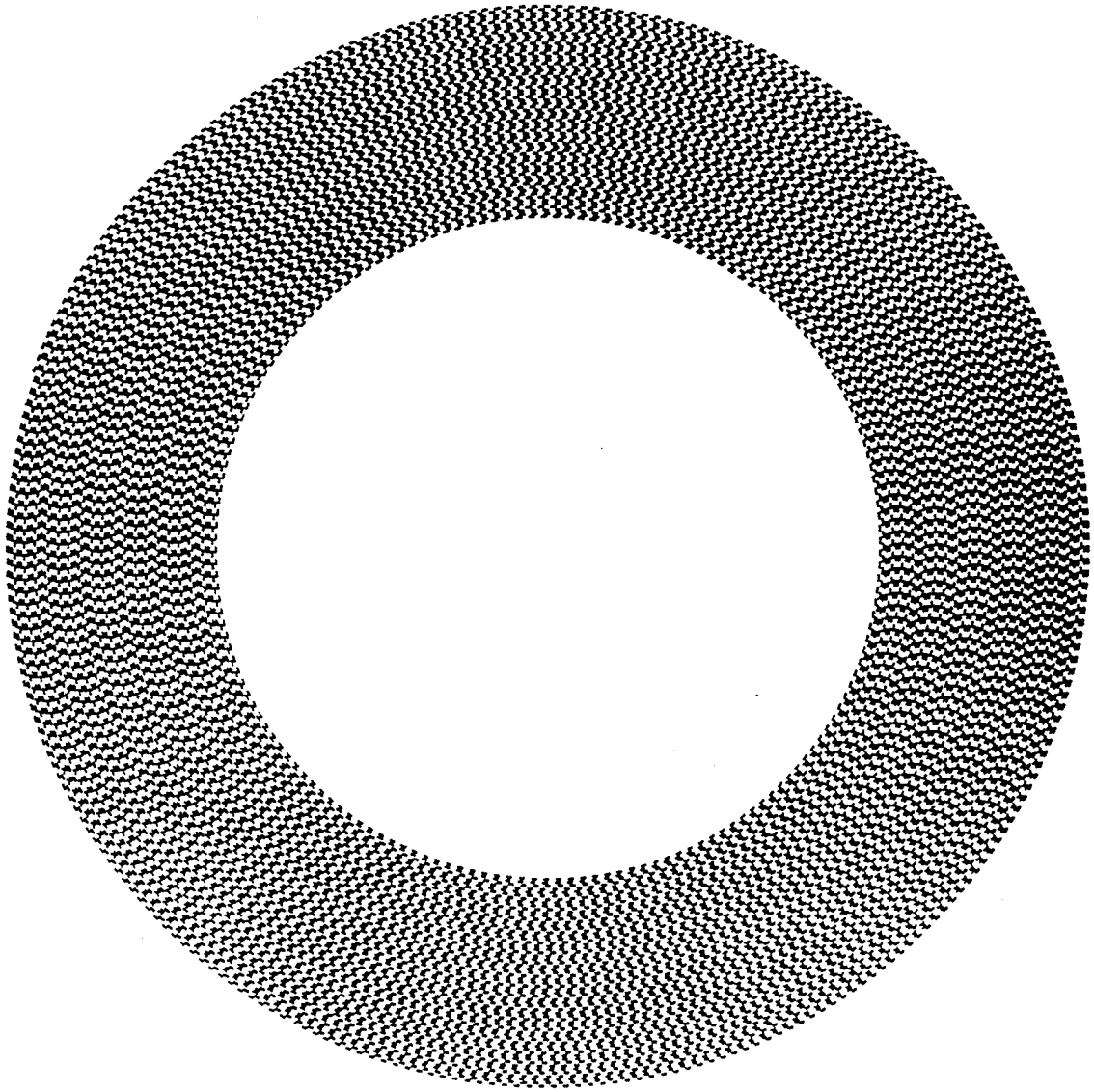

Fig. 14 A candidate scroll pattern for the SPRE regenerator (2/3 full-scale) in which the tape thickness is 0.027", wall thickness = 0.050", and gap thickness = 0.050".

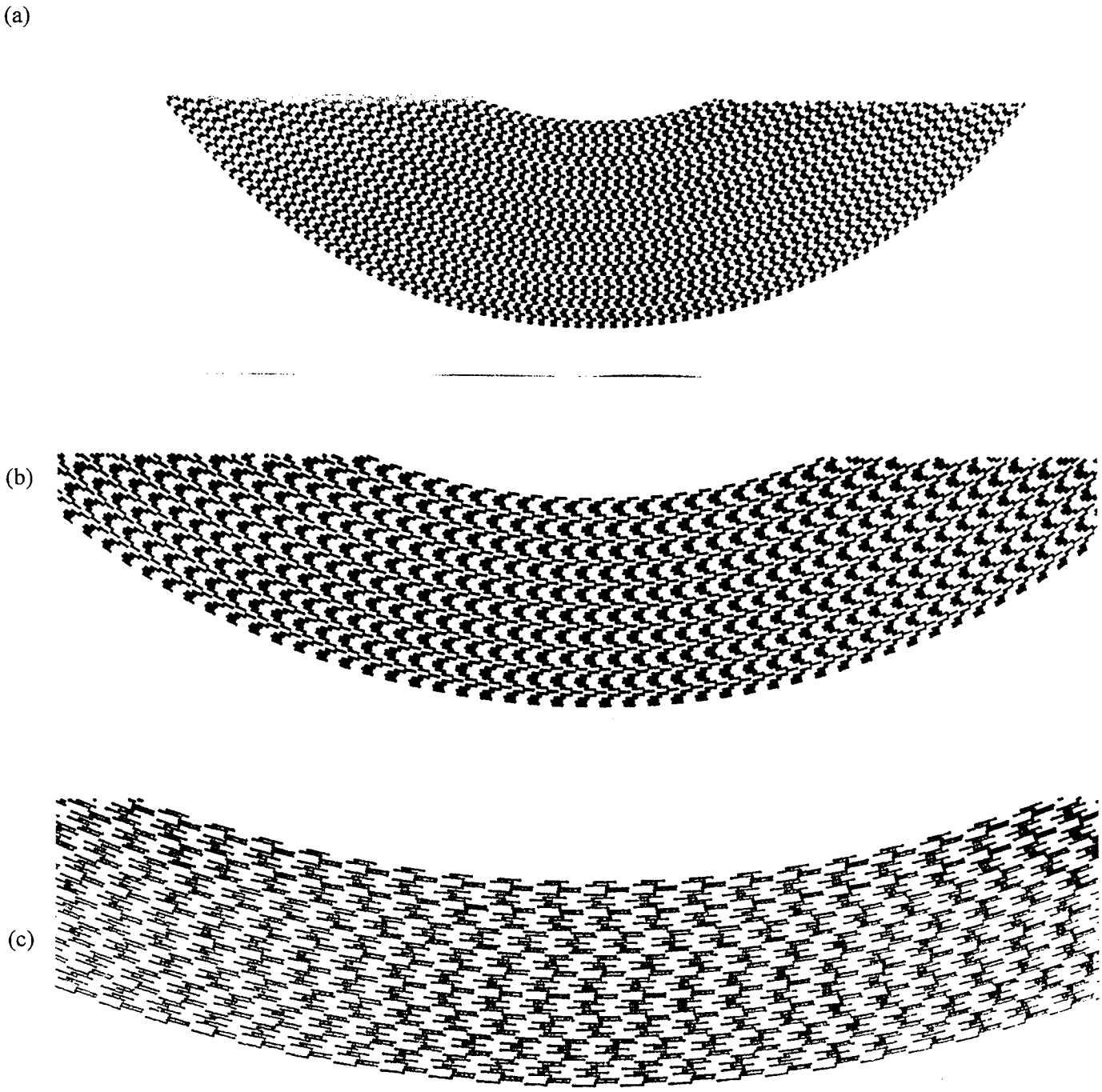

Fig. 15 Crescent-shaped flow channels in the scrolled tape regenerator for three different tape thicknesses (a) 0.027", (b) 0.013" and (c) 0.00675". Case (b) is shown at 2x magnification and case (c) at 4x magnification.

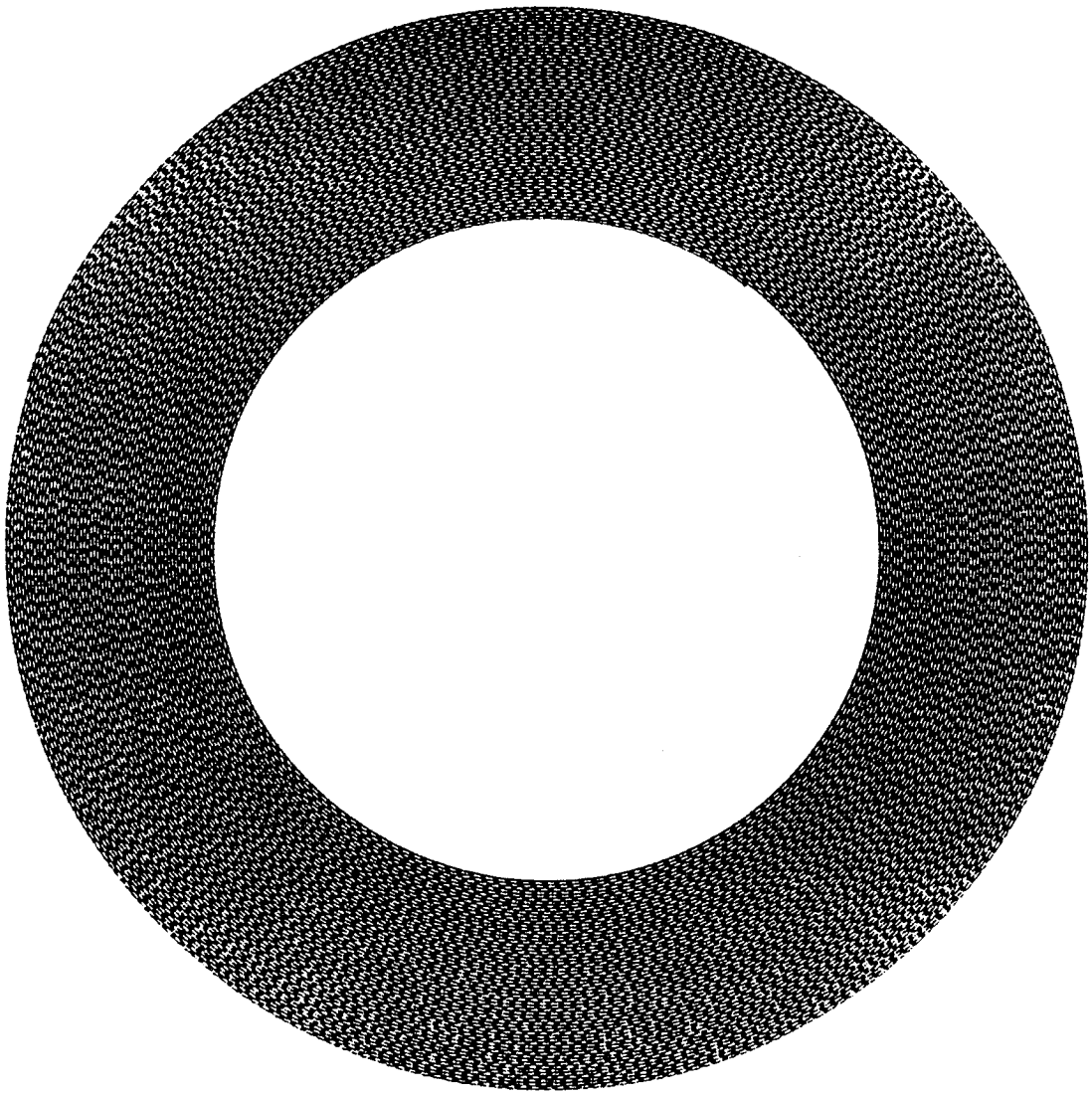

Fig. 16 Scroll pattern for SPRE regenerator (2/3 scale) formed with a bilayer scroll consisting of a 0.009"-thick solid tape wrapped with a 0.018"-thick slotted tape. The slot pattern has 0.100" pitch with 25% porosity.

Fig. 17 Detail of scrolled regenerator in Figure 16 showing slot pattern. Line thickness has become distorted in copying, so that the 0.009" walls appear thinner.

Tape applicator **Fig. 18** shows the applicator studied at ESLI to print carbon strips of suitable width and thickness onto unidirectional carbon fiber tapes. The take-up reel is scaled for the SPRE regenerator, but may be reconfigured for other annular regenerator types.

Stepper motors were set up to advance the tape and to raster a non-contacting applicator needle driven by a peristaltic pump. The tape advances one unit (2.5 mm, 0.10") and the applicator paints a line by passing across the tape; the tape advances another unit and the applicator returns painting another line. A sample of the pattern produced by a felt tip pen on a continuous paper tape is shown in **Fig. 19**. When using a carbonaceous adhesive slurry (Dylon cement) onto felt the definition of the lines was not adequate and the print-through was unreliable. The resin viscosity and felt porosity were such that a neat line through the felt thickness (0.25 mm, 0.010") was not achieved.

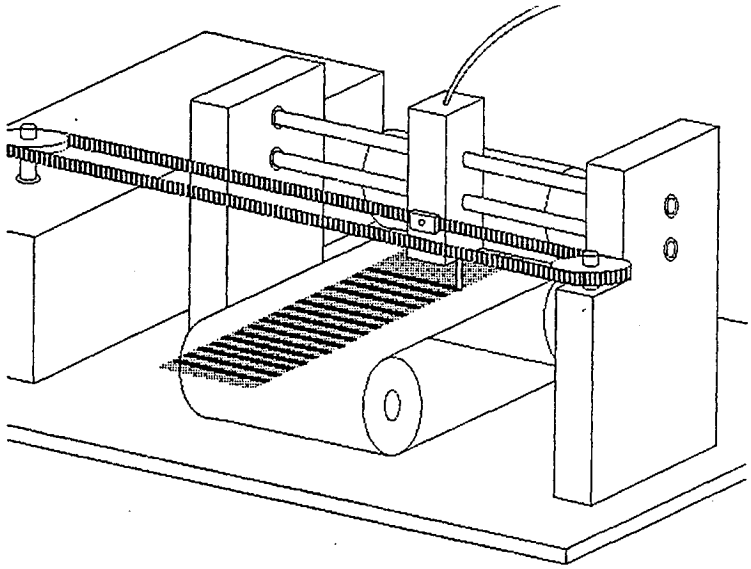

Fig. 18 ESLI tape applicator for printing stripes on unidirectional fiber tape.

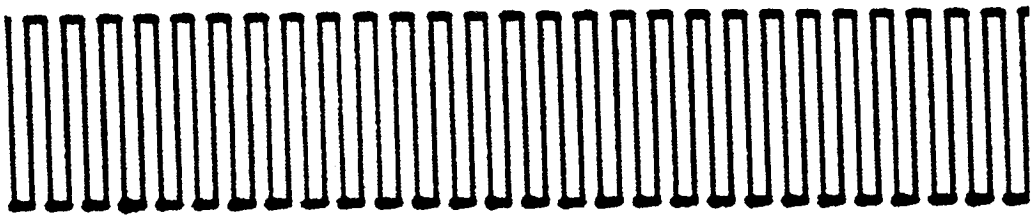

Fig. 19 Sample of continuous printing of line pattern on tape produced by automated tape printing system.

3.1.3 Flocking

Electroflocking - Electrostatic positioning of carbon fibers is promising as a low cost means of creating anisotropic conductivity structures. Flocking is a common textile technology and underlies the production of velvet and carpet-like fiber structures. There is very little information on the flocking of carbon fibers in the textile or composite materials literature [Kane, 1969; Cook, 1971], but ESLI had prior experience flocking discontinuous vapor-grown carbon fibers and pursued the method for regenerator fabrication. The process is shown schematically in **Fig. 20**. The fibers become charged at the source electrode and are forced by the electric field to move to the target electrode. The fibers orient parallel to the electric field because the induced dipoles are at lowest energy in this orientation. When an adhesive is applied to the target electrode, or to a film placed in front of the electrode, the arriving fibers stick and tend to remain oriented normal to the surface. Electric forces dominate the gravity forces and the orientation of gravity is not critical.

Different types of flocked structures relevant to heat exchanger design may be produced by this method as illustrated in **Fig. 21**. For regenerator applications flocking offers a means of orienting high-*k* fibers transverse to the flow direction, enabling composite regenerator design with parallel ducts that have transverse high-*k* carbon fibers to enhance heat transfer into the duct walls. Wider ducts can then be used which opens fabrication possibilities. High regenerator effectiveness requires flow channel widths not greater than 0.5 mm, so that a multiplicity of such channels are required for most regenerators (for example, at least two would be required for the HP-1000).

Precision cut high-*k* carbon fibers are not commercially available nor are means of cutting 10 g quantities of fiber tow to lengths 0.2-3.0 ±0.05 mm. A computer-controlled flock cutter was built that achieved a reasonable precision of flock with 0.2 mm and 2.5 mm lengths (**Fig. 22**). The flock cutter was equipped with stepper motors that advance the tow via pinch rollers into the blades (**Fig. 23**). The production rate is approximately 10 g/hr at 1 mm length. This modest capability meets requirements for this laboratory scale project, but a higher rate of production would presumably require replacing the slow scissor cutter with a faster rotary cutter mechanism.

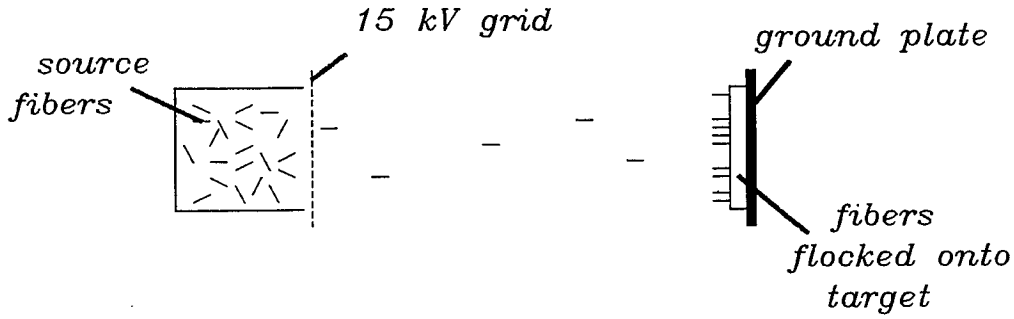

Fig. 20 Schematic electroflocker.

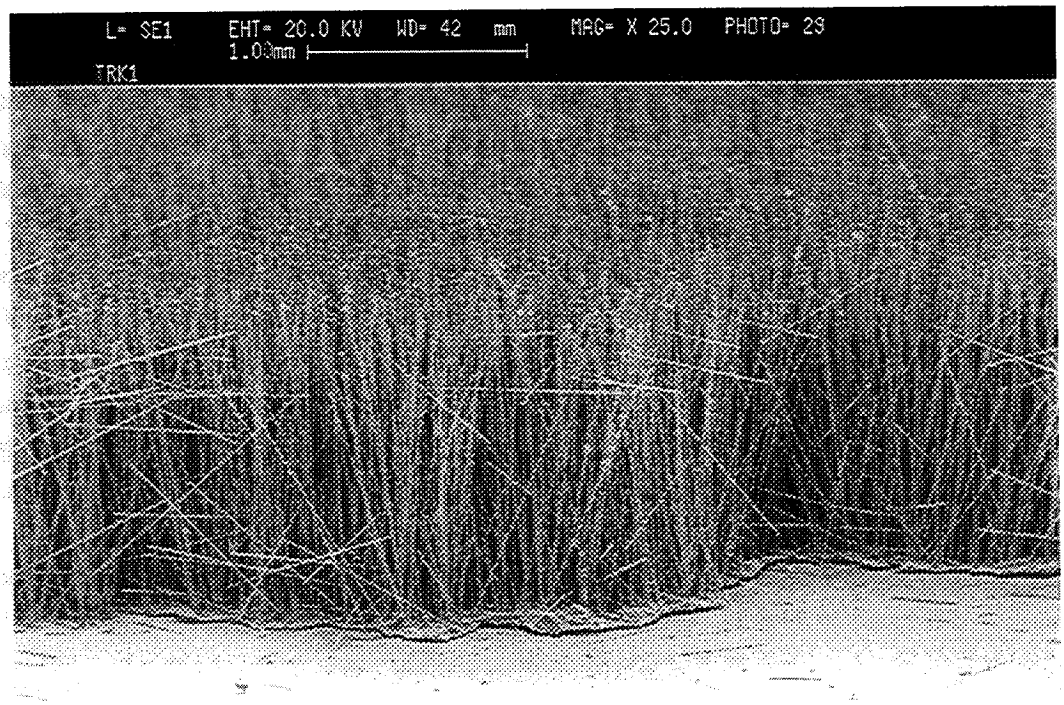

Fig. 21 Illustrative carbon fiber flocks.

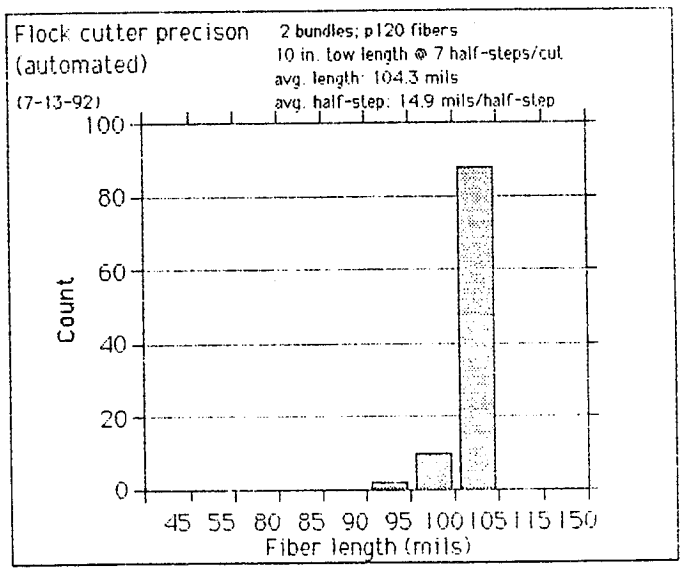

Fig. 22 Flock fiber length distribution obtained with the automated flock cutter.

(a)

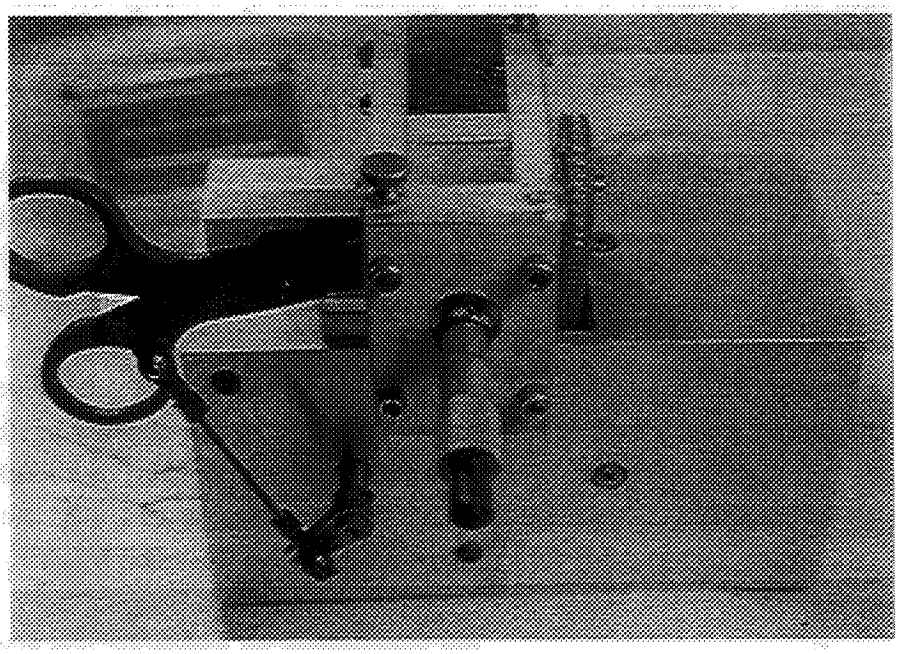

(b)

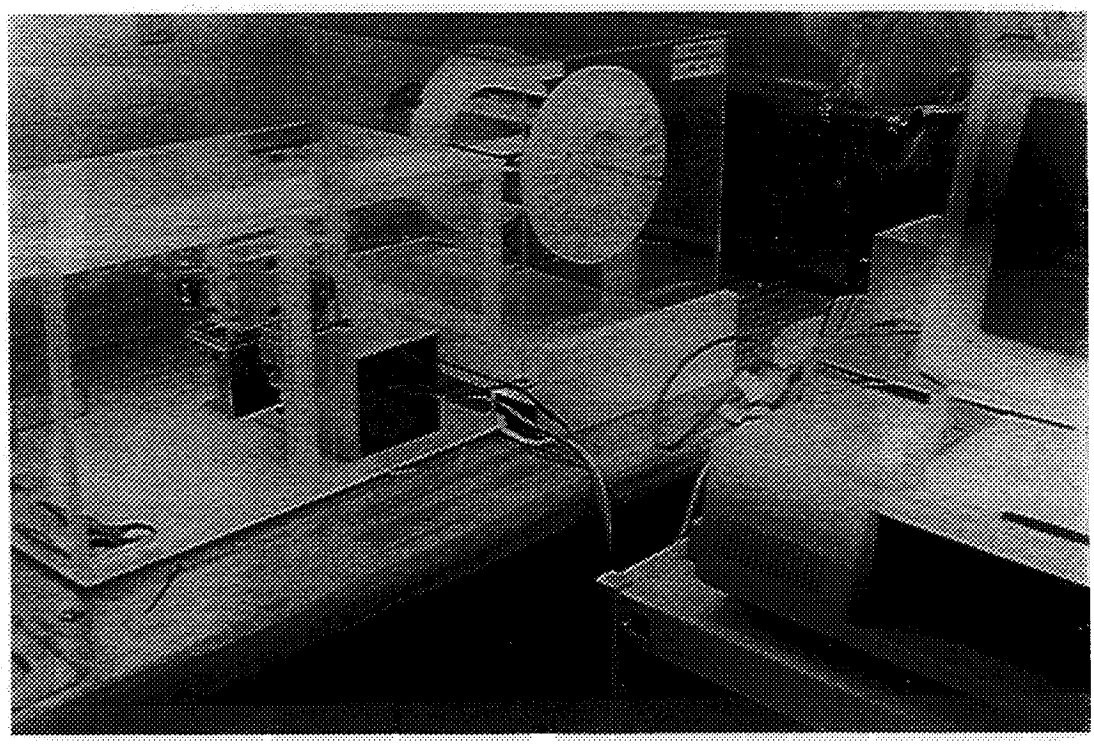

Fig. 23 Flock cutting hardware showing (a) cutting head assembly with micrometer stop and (b) automated cutter with stepper-motor control of flock length. Spread in length of cut flock appears to be within ±0.1 mm.

Flocked felt - Attempts were made to implant fibers by flocking into fabrics and felts. The concept pursued was to implant fibers into the felt and thereafter load the felt with a suitable carbon matrix. A carbon-carbon composite regenerator might then be fabricated with such a fuzzy layer, for example by scrolling.

The first experiments were performed flocking 1.2 mm long fibers into a 3k tow T-300 fabric comprising 24 warp tows/inch. This fabric had been heat treated to 2000°C prior to flocking and therefore was free of any sizing. No significant fiber penetration was observed and it appears that the fibers simply bounce off the fabric placed in front of the target electrode. Typical potentials used in these experiments were 10 kV over gaps of 1-5 centimeters.

The next experiments were conducted with lower density fiber targets. Flocking onto a carbon felt showed a limited amount of penetration (**Fig. 24**), but the quantity of fiber implanting deeply into the felt was not adequate. The weak implantation presumably is a result of the low fiber velocity which is estimated via strobe photography to be on the order of 1 m/s. Attempts to use higher field strengths to increase this velocity significantly were frustrated by charge leakage effects from the fiber tips.

Flocking into felt that has been partially impregnated with phenolic was attempted. An impregnation consisting of binder and carbon soot resulted in a dry green structure that is still flexible enough to be flocked and scrolled. Although the top of this felt could be flocked well with a fiber packing fraction ~3% , the fibers did not penetrate into the felt and attempts to merely press the fibers into the felt toppled them over.

Fig. 24 Short carbon fibers flocked on carbon felt at 3 kV.

Ceramic film - Carbon fibers were electroflocked onto an alumina film precursor that was wetted with alcohol to make the surface sticky. The fibers did not penetrate significantly into the film. The resulting fuzzy film was covered with another ceramic film layer that was heavily wetted with solvent to permit it to penetrate around the fibers. The resulting structure is shown in **Fig. 25**. The adhesion appears good.

Flocked Plate CMR Sample flocked channel structures were fabricated for testing. The pressure drop of the channel as measured indirectly by the time for flow of a specific quantity of fluid through the channel was compared to that of stacked screens and found to be approximately 10-fold lower. This is consistent with approximately 10-fold lower wetted area. This is the first example of carbon fiber flocked flow channels. The samples do not have the carbon fibers embedded in the walls; instead they stand on the walls with a thin (2-mil) adhesive layer holding them in place (**Fig. 26**).

Other flocked channel structures were prepared with high-*k* fibers partially embedded into a carbonaceous adhesive layer. The process used an aluminum plate with 0.025 inch thick rails. A boron nitride mold release was applied (also teflon film has been used). The plate and rails form a 0.025 inch deep trough which was filled with a carbonaceous adhesive from Dylan, which consists of approximately 30% phenolic resin, 20% furfural alcohol and 50% graphite. This layer was flocked with 2.5 mm long P-120 fiber. The flocked Dylan was cured for 4 hours at 100°C followed by 4 hours at 120°C. The cured Dylan layer was removed from the trough and the trough was

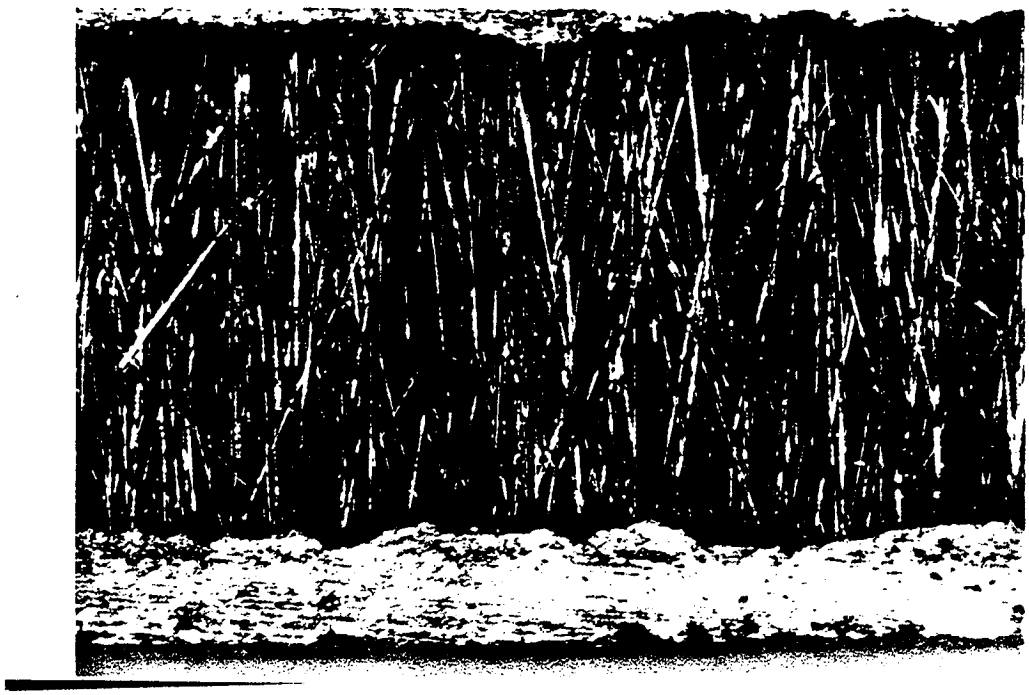

Fig. 25 Carbon fibers penetrating alumina film precursor (unfired).

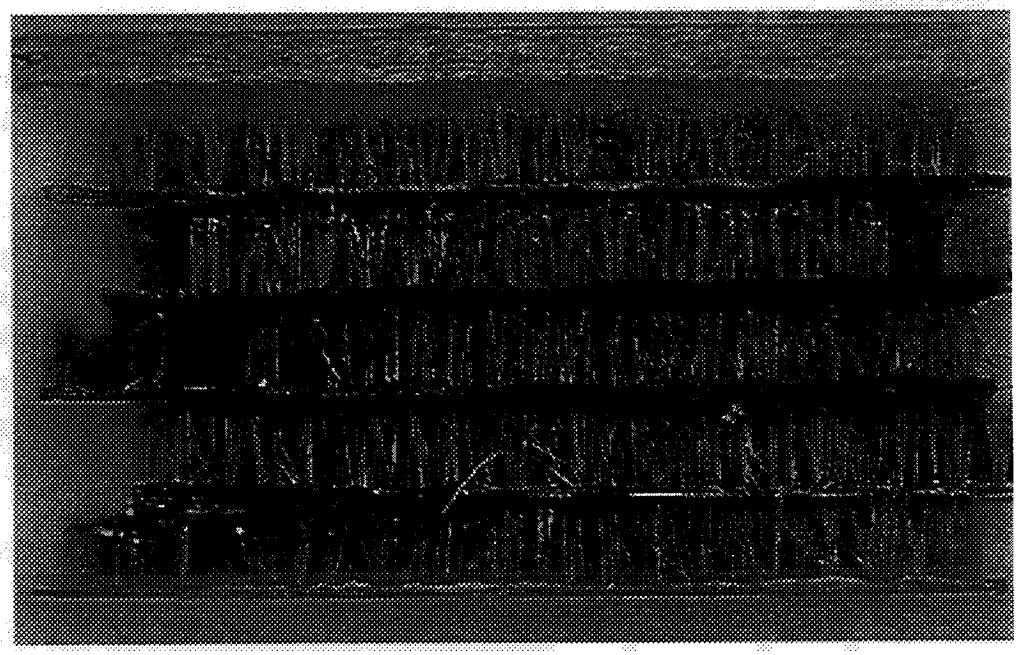

Fig. 26 Concept for flocked plates used in stack and wrapped configurations.

refilled with Dylan. The fiber side of the flocked, cured layer of Dylan was placed under light pressure (0.06 psi) into the Dylan filled trough. The final sandwich structure was then carbonized. Only partial penetration of the flock into the Dylan was achieved with modest pressure, and with higher pressure the flock collapsed. Attempts to thin the adhesive resulted in somewhat better penetration, but the cured layers were nonuniform in density.

Dual flock concept - In view of the difficulty of inserting flock into a suitable matrix, means of backfilling the matrix into a dual-height flock structure were investigated. Flocked tape structures that incorporate two fiber lengths were prepared (**Fig. 27**). This structure is produced by using a mixture of two flock lengths as the fiber feed stock in our electroflocking apparatus.

The expectation was that a fluid will wick into the short flock to form the desired plate, and the long flock will project out of this plate forming the channel pin fins in the CMR design. Such a dual-flocked tape can be scrolled forming an annular regenerator. A tape made with a mixture of 2.5 mm and 1.25 mm flock lengths would form a 2.5 mm thick tape whose width can be 10-30 mm or more. The side of the tape with high flock density would become the channel walls after impregnation by capillary effects. The flow channels would be 1.25 mm wide and contain a moderate density (5%) of high-k (1100 W/m-K) carbon fibers approximately 1.25 mm in width. The surrounding walls are 1.25 mm thick and are in good thermal contact with the channel because of the penetration of the long fibers. The majority of the heat capacity is contained in these walls that amount to approximately 50% of the regenerator volume. The thermal contact between this

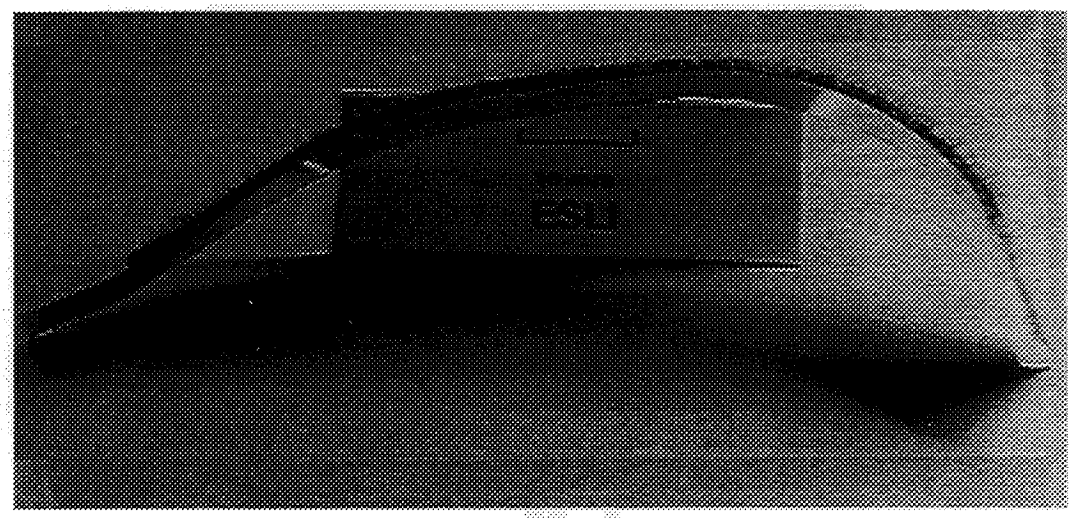

Fig. 27 Sample of dual flock structure, incorporating two flock lengths: the short fibers provide capillary retention of the matrix material and the long fibers provide heat conduction from the working fluid into the wall.

wall capacity and the working fluid strongly influences the regenerator thermal effectiveness.

A dual-flocked sample for testing in the single blow rig (Appendix A) was fabricated for testing as shown in **Fig. 28**. The flock was positioned on a thin adhesive layer and Dylon matrix was drawn into the short flock by capillary action. During cure, shrinkage and warping occurred, so that the final stacked structure has gap defects.

Wicking problems in dual flocks - The above concept has the defect that matrix material wicks up into the flow channel region wherever two or more fibers touch or are close enough together. It appears that resin also tends to pull fibers together and generate this problem. The net result is a channel structure in which a fraction of the carbon fibers in the channel are loaded with resin, reducing their effectiveness and increasing flow resistance.

In an effort to suppress the wicking of matrix into the channel flock, centrifugal processing was attempted. The speculation was that high enough centrifugation would drive the matrix where it belongs at the outer radius. The circular channel is consistent with annular plate design, and it is thought that if centrifugation works, an annular regenerator could be built up in successive layers.

The following process was attempted: a paper tape flocked with fiber is placed on the inner circumference of a graphite ring 15 cm in diameter that was placed on a centrifuge head assembly preheated to 160°C. A quantity of high temperature paraffin wax with MP $\approx$ 150°C is melted. The hot centrifuge head is placed on the centrifuge motor, rotated at 500 rpm, and the hot wax poured into the rotating head. The wax should flow under centrifugal force to the outermost radius,

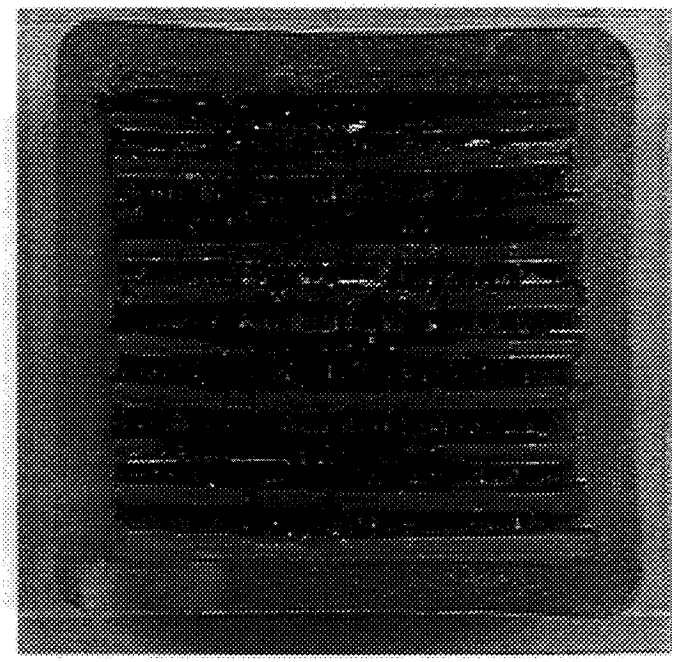

Fig. 28 First dual-flocked SBR test sample. The non-flatness and gaps at the sides are considered faults, but the test data will be useful for comparison purposes.

penetrating the flock. Cool down and wax freezing occurs while rotating at 500 rpm. The complete assembly is again reheated to 110°C, spun up to 500 rpm, and a calculated amount of carbonaceous matrix (mixture of phenolic resin, graphite powder and furfural alcohol) is injected into the center. While spinning, solvents evaporate leaving a viscous layer placed firmly in the flock against the wax layer. The assembly is then placed in a curing oven at 120°C. Once cured, another matrix layer is applied and the whole process repeated. Eventually the graphite ring is carbonized at 900°C, vaporizing all traces of wax and resulting in a carbon-carbon part ready for densification by vapor infiltration.

The concept was tested and a single fiber channel was produced. During cure the ring shrank and warped significantly. It may be that constraining forms could be used to achieve a more precise net shape without warpage, but this method appeared impractical. Continuing difficulties with wicking of resin into the channel regions and deformation of the resin matrix during carbon processing led to abandoning that approach.

Carbon vapor infiltration - To avoid the problems encountered using resins, carbon vapor infiltration (CVI) methods were investigated. The concept is to use CVI to densify a flocked preform to provide the necessary mass and heat capacity. A dual flocked preform could in principle be used, but CVI coats all fibers uniformly.

A modified design was therefore investigated in which an annular core of anisotropic graphite is used as a substrate upon which a radial fiber distribution is electroflocked and then densified with CVI carbon. This design differs from the basic CMR concept in that the fibers are

not used to transport heat to the channel walls. Instead the fibers are thickened to diameters 60-80 μm to provide the necessary heat capacity. This will be achieved by flocking 10 μm fibers and using CVI to coat the fibers to the desired thickness.

Compared to a felt or metal rope (Metex) design, the fibers are radially oriented. There is however a carbon wall supporting the flock whose thermal conductivity is an issue. A candidate material for this wall is Grafoil, oriented transversely so that the axial thermal conductivity is low. The standard HP-1000 regenerator has a steel wall supporting the Metex rope. The benefits of the carbon regenerator are expected to be:

- higher temperature capability (all carbon)
- lower axial conduction loss (lower axial thermal conductivity)
- lower pressure drop of radial fiber distribution

This type of regenerator, however, is not as tough as a steel regenerator and potential debris problems may occur in use.

Initial tests were encouraging in that precision shape and uniform coating were achieved. This method was used for the fabrication of the prototype HP-1000 regenerators, described in Section 3.5.

3.2 CMR Modeling

The fundamental goals of the modeling and analysis are a better understanding of desired regenerator characteristics, specific analysis of the CMR, and modeling of engine performance with the CMR *vs* conventional regenerators. The required compromise in regenerator design has long been recognized, but the first explicit closed form solution was done by Radebaugh and Louie (1984). Building on earlier work by Smith and others at MIT, they used a decoupled approximation of the losses in the regenerator. They showed several desirable features of Stirling cycle regenerators. Some of these desired features are, not surprisingly, constrained by practical design considerations.

Many approximations were made in this analysis. One is the assumption of linear addition of losses. A second is the standard problem in Stirling engines of using steady state correlations to analyze a complex transient thermofluid problem. The actual Stirling cycle has both oscillating flow and a pressure wave, combined with the unsteady thermal conduction in the solid regenerator material.

The starting point for the analysis is the performance of an idealized Stirling cycle. Various engine losses are then subtracted to give net power or refrigeration. These loss terms include regenerator ineffectiveness, pressure drop, and thermal conduction. Other terms are included at very low temperatures to model effects which are negligible at engine temperatures. The result is an expression for the net power (or refrigeration) of a Stirling cycle. Two fundamental results confirm earlier heat exchanger analysis: 1) the regenerator should be as large in frontal area as is consistent with conduction losses and design constraints; and 2) the regenerator should have the highest

possible ratio of heat transfer to pressure drop. For historical reasons arising from higher Reynolds number turbulent flow, the parameter used to characterize the heat transfer is the Colburn j-factor. It is divided by the Fanning friction factor, f, to give the figure of merit α. St and Pr are the Stanton and Prandtl numbers.

$$j = St\ Pr^{2/3}$$

Stirling engines usually have metal regenerators, such as screens, felts, or a rope-like weave made out of stainless steel. These structures perform well if properly sized for the engine being designed. However, they fall well short of the theoretical best structure, which are planar ducts. The planar ducts, in theory, will also outperform the originally proposed fibers in cross-flow. **Fig. 29** shows theoretical and experimental values of the figure of merit. The solid lines are the values from Radebaugh. The dashed lines are the experimental data from Pucci et al (1967). The symbols with solid connecting lines are our data (see Section 3.3.2 and Appendix A).

The difference between the standard correlations and measured values in Fig. 29 is interesting. Simple duct structures have higher figure of merit in theory, but planar ducts often do not perform as well as expected (Pucci et al, 1967), perhaps because of flow maldistribution. Also, experimental work on slotted foils (Pucci et al, 1967) and theoretical work (Amon and Mikic, 1990) predict that slotted planar ducts should have a higher figure of merit than planar ducts for certain Reynolds numbers. The slots serve as eddy promoters that increase performance. They also cut down on the axial thermal conductance and allow redistribution of flow between flow passages.

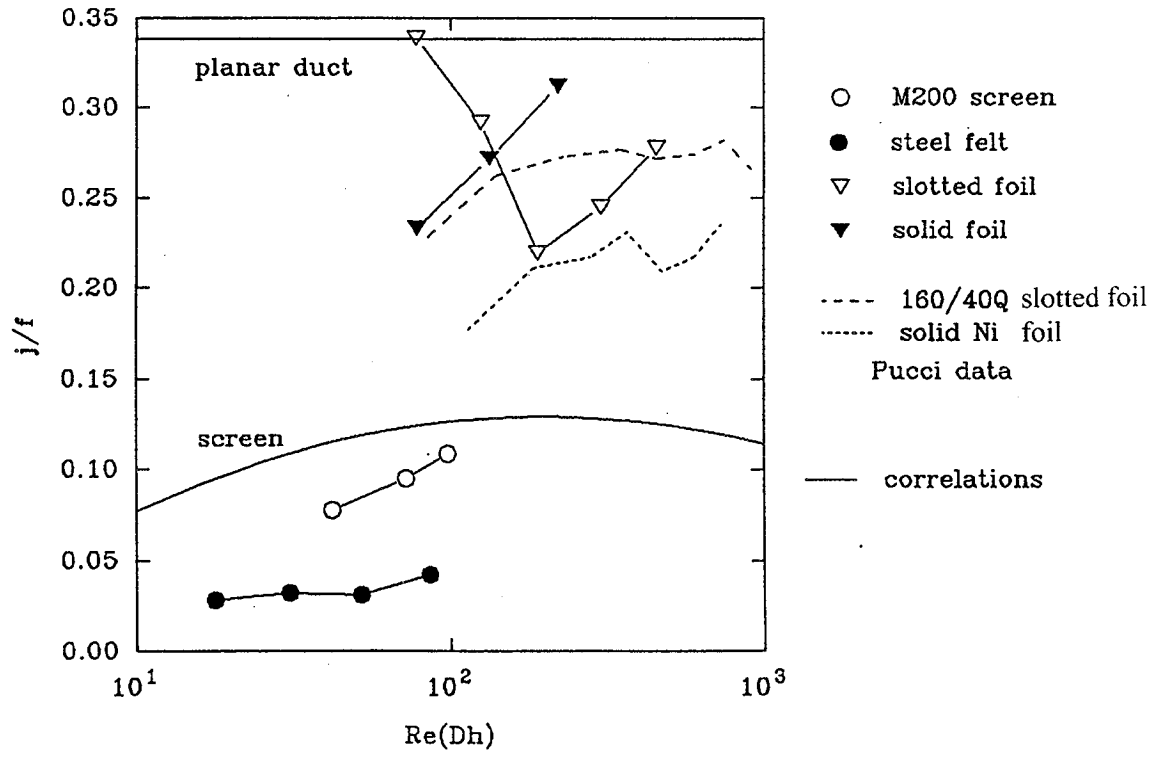

Fig. 29 Figure of merit α = j/f *vs* Reynolds number.

3.2.1 Fibers in cross-flow

Analysis of the performance of the CMR requires a model for the performance. We chose the simplest model consistent with a reasonable explanation of the observed data. The starting point is the heat transfer and pressure drop correlations for a single fiber in cross-flow. It is assumed that the fibers act independently. This assumption is probably reasonable at the fairly low fiber densities present in some of the experimental samples. At higher packing fractions, some type of tube in crossflow correlation might be more appropriate. The heat transfer correlation for the Nusselt number was taken from Kreith and Bohn (1986), "Principles of Heat Transfer", as originally presented in Zukauskas (1972). The correlation for the average Nusselt number is given as a function of the Reynolds number and the Prandtl number. The correlation is shown in **Fig. 30** as "Nu" for Pr = 0.71, e.g. nitrogen at atmospheric conditions. The correlation changes at Re = 40, which shows up as a slight kink in the graph.

The drag coefficient, which is equal to the Fanning friction factor for exterior surfaces like cylinders, was extracted from the graphical plot of Hoerner (1968) labeled "Drag". Points were measured at each decade of the Reynolds number from 1 to 1000. The points obtained were then fitted to a third order polynomial. This produced a smooth plot passing very near to each of the original data points. This correlation is labeled "f" in Fig. 30. The graph shown at the bottom of Fig. 30 is the figure of merit $\alpha = j/f$ which has a broad maximum of 0.069 at Re $\approx$ 3 and drops to 0.0148 at Re = 1000.

The correlations above represent an upper bound on the effectiveness for the actual geometry in which heat is conducted down the carbon fiber and into the wall. An estimate of the conduction effect may be made using "pin fin" analysis as presented in Kreith and Bohn (1986). In this analysis, one assumes that each fiber acts like a pin fin whose length is one-half the channel height and symmetry allows the tip to be treated as adiabatic. Also one may assume as a first approximation that the fluid is isothermal (this assumption is relaxed below).

The formula in Kreith and Bohn (1986) can be rewritten in terms of the Nusselt number and the ratio of the gas to solid thermal conductivities. It gives the result in terms of the parameter x, where L is the pin fin length (one-half the channel height), D is the fiber diameter, Nu is the average Nusselt number, and k is the thermal conductivity, where subscript s denotes the solid (fiber) and subscript g denotes the gas:

$$x = \frac{2L\ (k_g/k_s)^{1/2}}{D}$$

$$\eta = \frac{\tanh(\ x\sqrt{\mathrm{Nu}})}{x\sqrt{\mathrm{Nu}}}$$

The efficiency is defined as the ratio of the heat transferred out of the fin to the heat transferred if the fin had infinite thermal conductivity. The efficiency drops with increasing x and Re.

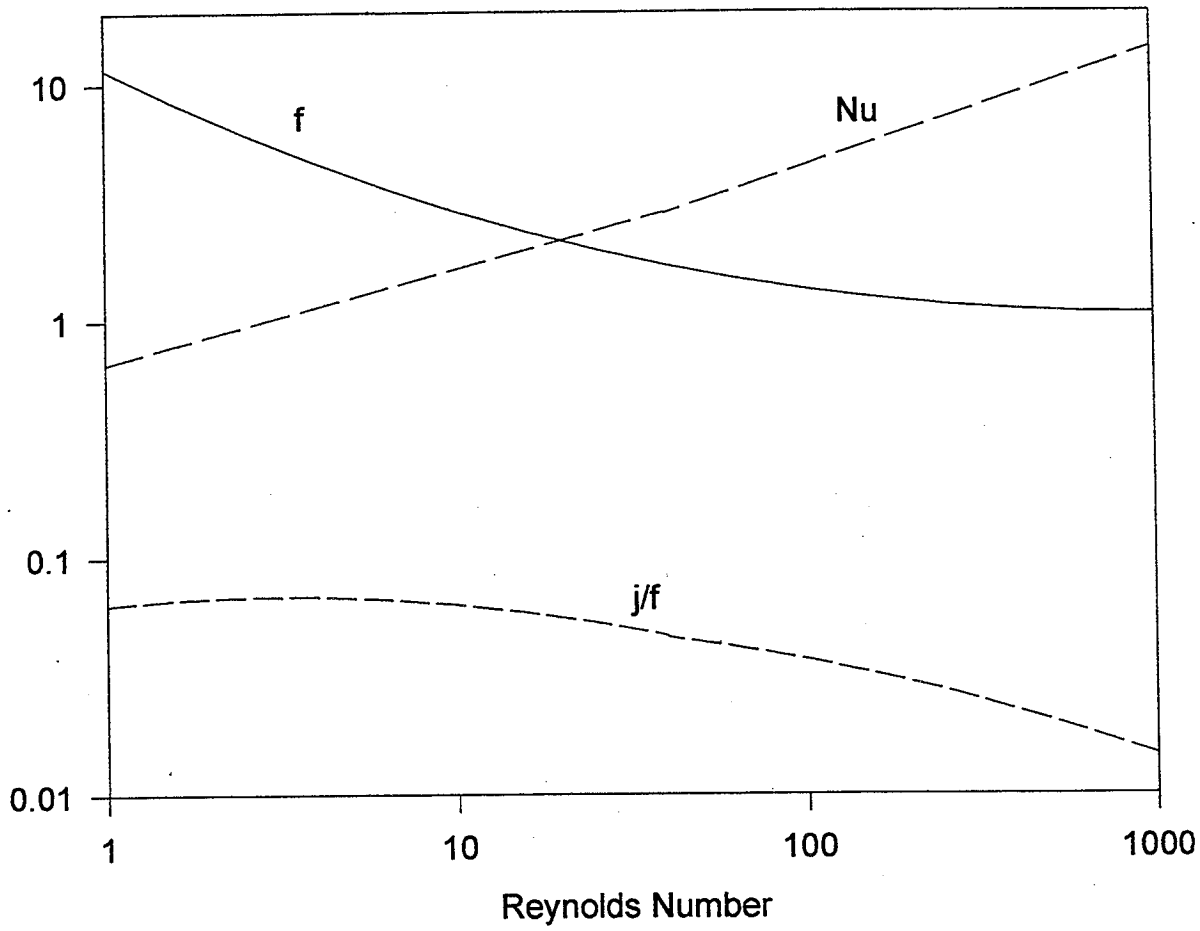

Fig. 30 Heat transfer & pressure drop correlations for cylinder in crossflow.

One can solve for the the temperature distribution in the fluid and drop the above assumption of isothermality. A simple solution was found for fully developed flow in the usual case where the heat flux at the base of the pin fins is constant. The symmetry allows the following assumptions:

(1) the temperature profile along the pin fin is independent of position along the channel; the baseline for this profile is shifted according to the fluid temperature rise along the channel

(2) the heat flux outward from the pin fin is constant at every point along every fin (constant temperature difference between fin and fluid)

The solution has a simple *quadratic* rather than *tanh* dependence on position along the fin. Of course, the baseline pin fin temperature rises linearly with position along the channel (in accordance with the bulk fluid temperature rise) and the fluid has a constant temperature difference everywhere with respect to the fin.

Practical situations seldom have fully developed flow. A 2-D numerical solution was developed to compute the general case, giving the standard pin fin result at the entrance, and the fully developed flow case in the asymptotic limit of a long channel. Solving for the heat transfer and temperature profile along the length of the pin fin at a given location x, these temperatures are used for the fluid temperature at the next grid position along the heat exchanger at point $x + dx$. The procedure then marches through the entire length, starting from the initial fluid input temperature. A matrix solution is desirable at each step to solve for the pin fin temperature profile, which is simply a standard tridiagonal matrix solver in the 1D flow geometry of interest. The numerical solutions can be compared to the two analytical solutions for (1) the entrance region and (2) the far downstream solution. The 2-D version agrees with the 1D pin fin model in the entrance region and it agrees fairly well with the quadratic fully developed flow solution. The small discrepancy likely results from either an insufficiently long channel or a discretization error.

The model is set up as a constant flux boundary condition at the solid walls, and has not been run with the boundary conditions appropriate to a regenerator.

Experimental results - A preliminary analysis of the flocked plate structure was carried out. For pressure drop the fibers are assumed to act like independent cylinders in crossflow. For heat transfer each fiber is treated as a pin fin. The predicted pressure drop was 0.3 psi, compared to the 0.5 psi pressure drop measured on the SBR sample (see Section 3.3.2). The predicted NTUs, including pin fin efficiency, was about 4% more than the measured NTUs and therefore within the experimental error.

3.2.2 GLIMPS/CMR Modeling

GLIMPS was purchased and used as the primary tool for engine modeling for this contract. GLIMPS (GLobally IMplicit Simulation) is a numerical Stirling cycle thermal model developed by Gedeon Associates. It models Stirling engines, heat pumps and coolers, describing them as seven

components (compression space, cooler heat exchanger, cooler manifold, regenerator heat exchanger, heater manifold, heater heat exchanger, and expansion space). The fluid and heat flows are assumed to have 1-D spatial variations. Characteristics of the working fluid interaction with the various heat exchangers are treated by use of correlations for the flow friction and heat transfer rate. The gas continuity, momentum and energy equations are solved at discrete spatial nodes along the components and for discrete time nodes during the cycle. A design point equilibrium solution is obtained, so that one cycle period contains all the information provided by the simulation.

For GLIMPS v4.0 David Gedeon incorporated features that allowed us to simulate the behavior of a CMR. One could modify the heat transfer correlations and materials properties in GLIMPS v4.0. A methodology for approximating the performance of the fibers in cross-flow was developed. The method assumes the pin fin approximation, as described above, as the input to the user defined correlations in GLIMPS v4.0. Because of the simpler functional form used in GLIMPS, the method requires some pre-fitting or reformulation of the above correlations for the relevant Reynolds number range of the machine being modeled. The separate problem of correctly modeling the solid conduction aspect of the problem is done as a separate calculation to ensure that the dispersion of the high-k fibers inside the wall is sufficient to allow good thermal penetration during each half cycle of the machine.

The additional capacity of the wall is modeled, if needed, by giving the solid regenerator material an artificially enhanced heat capacity. Combined with the ability to separately vary the two components of the thermal conductivity in the regenerator, this provides the necessary flexibility to model the performance of a composite regenerator, subject to the thermal penetration check calculation described above. For a simple planar duct, the problem is straightforward and only requires the thermal anisotropy. However, for the fibers in cross-flow, the technique requires that, as seen by GLIMPS, the only available capacity volume is the regenerator solid material actually embedded in the flow passages. The extra heat capacity of the wall is simulated by increasing the heat capacity of the fibers in the flow by the ratio of the mass of the wall material to that of the fiber material. A justification for this simplifying assumption is that the radial carbon fibers have high thermal conductivity, but the correctness of this assumption is not understood. Appropriate adjustments to correctly model the thermal conduction loss in the solid regenerator wall are also taken care of by using a consistent procedure to artificially increase the axial thermal conduction loss.

Ross D-60 GLIMPS simulations - GLIMPS runs were set up using the driver program VARY to do multiple runs while varying a single parameter. The results are shown in **Fig. 31**, plotting PV power *vs* frequency. Runs were done for the following stainless steel foil regenerators: (1) 0.001" foil, 0.0073" gap; (2) 0.002" foil, 0.006" gap; (3) 0.001" foil, 0.003" gap; (4) 0.003" foil, 0.003" gap; (5) 0.002" foil, 0.002" gap. The regenerators are listed with the highest power first. The results of the modeling are substantially different from the measured performance, although at 35 Hz they are in reasonable agreement (see Section 3.4 for test results).

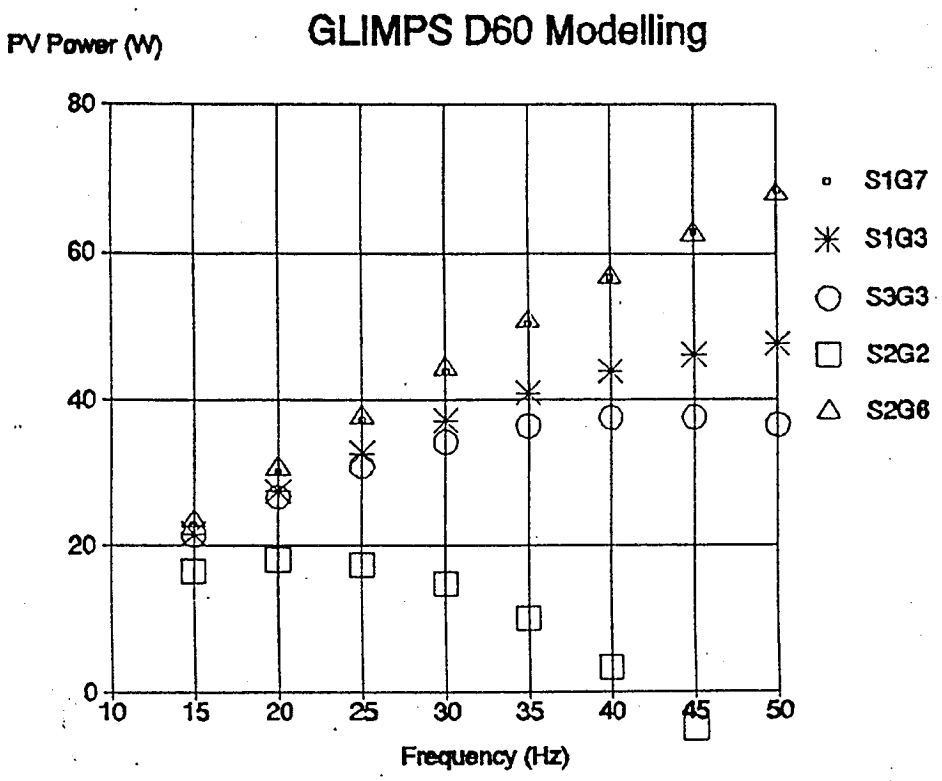

Fig. 31 GLIMPS modeling of Ross D-60 engine.

HP-1000 modeling - GLIMPS modeling of the HP-1000 engine was done using an input file provided by Steven Geng of NASA Lewis Research Center. The steel Metex regenerator was replaced by a carbon regenerator. Note that this is not a composite matrix regenerator. Constant properties for the carbon were assumed: thermal conductivity of 20 W/m-K and specific heat capacity of 711 J/kg-K. The carbon density was assumed to be 2 g/cc. GLIMPS uses a steel volumetric heat capacity about three times higher than the carbon values given above.

Runs were done by changing only one parameter at a time. The nominal design, with steel, has a PV power of 918 W. With the nominal carbon regenerator the power is 864 W. For comparison, runs were made with carbon heat capacity of 0.5 and 10 times the nominal values, giving powers of 789 and 938 W respectively. The carbon regenerator wire diameter was varied from 70 to 100 μm, from the original value of 88.9 μm (**Table 5**). The diameter 80 μm was selected as the nominal wire diameter for the thickened carbon regenerator, since there was very little gain in going above 80 μm to warrant the additional deposition time.

The regenerator frontal area was varied for 80-μm diameter wire and the results are shown in **Table 6**. A nominal area of 16 cm^2 was selected as giving a reasonable improvement without too large a change in the area. A final run, done with a shorter regenerator length of 3.5 cm, yielded the results shown in **Table 7**. Due to the complications of changing the regenerator length in the fixed size canisters, the nominal length was left unchanged at 4.445 cm. A shorter, fatter steel regenerator also showed better performance, increasing to 943 W from the original 918 W.

Pressure drop measurements were done on the sample HP-1000 regenerator canister with the Metex 3.5 mil diameter material. The measurements were done with dry nitrogen gas at ambient exit pressure, as with all other measurements done in the project. A new fitting was made to allow connection to the 1" I.D. tubing used in the flow path. The results were converted into Fanning

friction factor as a function of the Reynolds' number, based on hydraulic diameter. The results are shown in **Table 8**.

Table 5 GLIMPS power *vs* wire diameter.

Wire diameter (μm)	Power (W)
70	861
80	865
85	865
88.9	864
100	861

Table 6 GLIMPS power *vs* frontal area.

Area (cm^2)	Power (W)
13.92	865
16	877
18	879
20	879
24	870

Table 7 GLIMPS power *vs* frontal area for 3.5 cm length.

Area (cm^2)	Power (W)
13.92	865
16	888
20	895
24	891

Table 8 Measured Fanning friction factors.

Reynolds Number	Fanning friction factor
71.4	3.26
119	2.38
196	1.79

For comparison, the Fanning friction factor at a Reynolds number of 196 is 0.932 in REGEN (code based on Radebaugh and Louie (1984) and offered by NIST-Boulder) and 1.032 in GLIMPS. Thus, the measured values from the single blow rig are substantially higher than the standard correlations.

The standard pulsed single blow heat transfer experiment was also done using the HP-1000 Metex regenerator. The resulting heat pulse was so spread out and diffuse that it could not be resolved from the normal background drift of the gas temperature. This was not too surprising, in view of the much larger than optimum thermal length and mass of the regenerator, compared to the small samples for which the single blow rig works best.

3.2.3 Composite regenerator channel width analysis

An analysis of an acceptable channel width for the HP-1000 composite regenerator was done using the pin fin analysis. There is some arbitrariness in the decision on what degradation of heat transfer is acceptable. It is assumed that the average temperature drop due to the thermal resistance

of the fibers is less than the temperature difference between the gas and solid. To do so for the HP-1000 requires a channel width of 0.5 mm or less. The composite regenerator was never built because of the difficulties in fabricating the required multiple small channels.

3.3 CMR Property Determination

3.3.1 Fiber strength

We investigated the question of whether brittle high-*k* carbon fibers can survive the high speed gas flow environment. It is possible that large channel widths will not support the fiber well enough and excessive breakage and fiber debris may result. Initial tests were performed with fibers spanning gaps of size 0.060", 0.050", 0.040" and 0.020" in high pressure dry nitrogen flowing across the fibers. Some fiber breakage was observed at the highest gas flow rates, although results were generally encouraging. Groups of several fibers bonded together with resin were observed to be quite strong and showed no breakage under the flow conditions tested. Fibers that are thickened by vapor infiltration are comparatively very strong and are not expected to break.

Amoco P-100 and P-120 carbon fibers were bonded with super glue across a 0.050" gap between two graphite plates. The fiber/surface interface was visually inspected at 30*x* power and fibers were selected for observation. The survivability of fibers having a free end was also tested. A row of approximately 20 P-100 carbon fibers was bonded with super glue to a pyrolytic graphite plate having a sharp edge. The fibers protruded past the plate and the free ends were trimmed to produce lengths varying from 2 mm to 5 mm. A polypropylene tube with a 0.12" orifice was held 0.2" from the fibers and used to direct a jet of dry nitrogen at the fibers. The maximum flow rate was 2.0 SCFM, corresponding to a flow velocity 130 m/s across the fibers. The dynamic pressure or velocity head $\rho v^2/2$ is higher in this testing than in either the HP-1000 or the SPRE, so that both potential cases are covered. The results on breakage are shown in **Table 9** where it may be seen that the more brittle P-120 fibers break at shorter lengths. All the lengths tested for both types of fiber have enough flexural strength to survive steady flow conditions more severe than those in the engines. The results in Table 9 also show that longer fibers with free ends break at lower dynamic pressure, as expected.

3.3.2 Single Blow Rig Testing

A pulsed single blow rig test method (SBR method) was developed for testing regenerator materials. The experimental setup and modeling techniques used are described in the IECEC paper by Oldson, Knowles and Rauch, included as Appendix A. A brief description is presented here. Compressed nitrogen from a regulated cylinder flows through a mass flowmeter and into a tube containing the regenerator material. Thermocouples and pressure taps are located just upstream and downstream of the sample. A fine mesh heater is located upstream of the temperature sensor to provide a heat pulse to the gas stream.

Table 9 Break length of carbon fibers in gas flow.

Fiber length (mm)	Flow rate at fiber break (SCFM)	(L/s)	Flow velocity (m/s)	Dynamic pressure (kPa)
P-100 Fibers, free end				
4.70	1.20	0.5663	77.7	3.771
3.81	1.40	0.6607	90.6	5.133
3.35	1.55	0.7314	100.3	6.292
2.79	1.80	0.8494	116.5	8.485
2.06	2.00	0.9438	129.5	10.476
P-120 Fibers, free end				
2.44	0.80	0.3775	51.8	1.676
2.01	1.00	0.4719	64.7	2.619
1.52	1.25	0.5899	90.6	4.092
P-120 Fibers, both ends fixed				
1.27 (gap)	1.40	0.5899	90.6	5.133

The shape of the pulse is recorded by the upstream thermocouple. The pulse shape is modified by the interaction of the heated gas with the regenerator sample, and is recorded by the downstream thermocouple. The pressure drop characteristics of the sample are measured by the pressure taps, which feed a differential manometer.

Interpretation of the results requires the use of a 1-D modeling program, also described in Appendix A. The assumptions are

- 1-D steady flow; 1-D temperature distribution
- gas divided into layers (slugs) moving at steady velocity, constant density (small T changes)
- no heat conduction between gas layers
- conduction between regenerator layers
- layers of gas exchange heat with equal layers of regenerator material
- test sample porosity and solid surface area are taken to be the nominal values

The need for numerical curve fitting is a major drawback compared to the technique of Pucci (1965), where a step increase in temperature is applied to the gas flow and analytic data reduction is used. However, the heater construction is much simpler for the pulsed method.

For some samples, the technique gave very good results. The paper shows two examples of clean data with good fits. In other cases, however, the data is poorer, and it is impossible to get a

good fit. The method does require that the sample be in a restricted range of NTUs to allow a good fit to be made. It also requires that the sample have a uniform effective passage size.

The results for the SBR specimens tested are summarized in **Table 10**. Because of the time required to do the matching of the experimental and modeled data, not all samples were modeled for thermal performance. In addition, some samples, such as the grafoil sample, were modeled but could not be fitted very well with our current modeling technique. In other cases, such as the packed alumina balls, the data appeared unusual, and no modeling attempt was made.

HP-1000 carbon regenerator testing and analysis - Single blow rig testing and modeling was performed on the extra carbon regenerator, fabricated as one of four for the HP-1000 Stirling engine at NASA Lewis. Earlier in the project, pressure drop testing had already been done on the four regenerators. Thermal testing had been attempted as well, but as expected, the thermal length of the regenerators was too long. In the single blow test method, a sample that is too long will completely disperse the incoming thermal pulse, and extraction of heat transfer properties cannot be done.

Since thermal test data were desired, it was decided to cut the last regenerator sample to a shorter length to enable thermal testing. This was done using a razor blade and saw, with an appropriate jig to hold the regenerator. The regenerator is fairly strong after carbon CVD, but the technique worked fairly well. The sample length as cut was 0.52 inches long. A shorter sample holder for use in the test rig was also fabricated.

Table 10 SBR test sample specifications and fitting parameters based on the SBR model.

	Name	Form	Re(Dh)	α=j/f	Filename	Diameter (in)	Length (in)	Volume (cm^3)	Mass (g)	Density (g/cm^3)	Porosity	Channel (μm)
Carbon/carbon	Coarse CC	slotted				1		0.000			50	762
Carbon/carbon	Fine CC	slotted				1		0.000			50	406
Stainless	Brunswick	felt				1	0.25	3.218		7.9	84	12.7
Stainless	Metex	wire knit				1	0.5	6.435		7.9	80	88.9
Cordierite	Cordierite	sq. channels				1		0.000				
Stainless	Brunswick	felt	51.7	0.035	br125m	0.75	0.255	1.846	2.61	7.9	82.18	25.4
Stainless	M200 mesh	stacked screens				0.75	0.39	2.823	9.09	7.9	67.01	53.34
Stainless	M200 mesh	stacked screens	72	0.082	scr26m	0.75	0.184	1.332	4.29	7.9	67.01	53.34
Alumina	Packed balls	balls				0.75	0.435	2.823	6.9	3.96	45	754
Carbon	Felt	felt				0.75	0.428	3.149	0.4	1.57	91.8	13
Carbon	Felt	felt				0.75	0.5	3.620	0.967	1.57	82.98	13
Vectra	LCP-1	corrugated				0.75	0.4	3.099	1.559	1.4	61.64	152
Vectra	LCP-2	corrugated				0.75	0.4	2.896	2.272	1.4	44.02	63.5
Stainless	Foil	corrugated				0.75	0.5	2.896	14.38	7.9	49.68	50.8
Stainless	Foil	corr. & slotted	179	0.0419	cpt30a	0.75	0.5	3.620	12.13	7.9	57.55	50.8
Glass	CGT	tubes	1118	0.068	cgt7a	0.75	0.5	3.620	6.17	2.23	48.8	838
Polyimide	CPT	tubes				0.75	0.5	3.620	1.37	1.42	40.7	254
Carbon/Wax	Flocked wax	stacked flock				.61 x .61	0.5	3.049	1.552		51.4	762/10
Carbon/carbon	Printed felt	graphite/carbon				0.75	0.5	3.620	0.84	0.232	93.92	152.4/10
Carbon	Scrolled felt	carbon	31.6	0.0297	spf7m	0.75	0.5	3.620	0.220	1.57	96.13	13
Carbon	Grafoil	carbon		no fit	gra7j	0.75	0.25	1.810	1.83	1.8	43.9	76.2
Stainless	Etched foils	spaced	191	0.219	efc19m	.61 x .61	0.5	3.049	9.24	7.9	60.5	101.6
Stainless	Foils	spaced	134	0.272	sp26j	.65 x .665	0.51	3.612	12.71	7.9	55.5	101.6
P120/Dylan	Flocked Dylan	Flock	2318	0.0195	flo21j	.61 x .61	0.5	3.620		1.34	0.6913	25.4
P120/Dylan	Flocked Dylan	Flock	1467	0.023	fl203s	.61 x .61	0.5	3.620		1.34	0.543	12.7

Testing was performed on the sample at nominal pressure drops of 0.5, 1, and 2 psi. The results, including the modeling used in data reduction are shown in **Table 11**. The pulse data for two individual test runs are shown in **Fig. 32**. Because of the apparently low thermal performance of the 0.52" long sample, the longer sample left after cutting the original 1.75" long sample was also tried. This sample, like the original one, was excessively long, and a useful output pulse could not be observed.

The hypothesis for this puzzling behavior is the effect of the high thermal conductivity carbon fibers leading to a large thermal mass. The problem is the time scale of the pulse, approximately 0.5 seconds, which is long enough for thermal conduction into the more massive carbon core to occur and distort the pulse, as well as invalidate the 1D model used for earlier sample data analysis.

Because of this, a two dimensional version of the model developed during Phase II work was developed to examine the effect of the high heat capacity wall on the thermal pulse. This 2-D model includes lateral conduction to the thermally large carbon core, modeled as a single node of very large heat capacity. The 2-D model, which was done with isotropic conduction for ease of coding, can qualitatively duplicate the pulse dispersion for the longer samples, but cannot, with the same parameters, allow the shorter sample output to be modeled well. An anisotropic thermal conductivity appears to be needed to more accurately model the process.

The results show a fairly low thermal performance, if correct. The figure of merit, alpha, shown in the last row of the Table 11, is the Colburn j factor divided by the Fanning friction factor. Typical measured values for α for standard regenerators are much higher than the values shown here. Alternate explanations are that either the modeling used in data reduction or the testing were in error. It has already been noted that the model does not correctly explain the disappearance of

Table 11 Test data and modeling results for shortened carbon regenerator specimen.

Pressure drop (psi)	0.50	1.00	1.99
Mass Flowmeter (volts)	1.087	1.750	2.690
Flow velocity (m/s)	4.431	7.133	10.964
Re (Dh)	131	211	325
Stanton	.02	.02	.016
Fanning friction	2.019	1.558	1.312
α	.0078	.0101	.0096

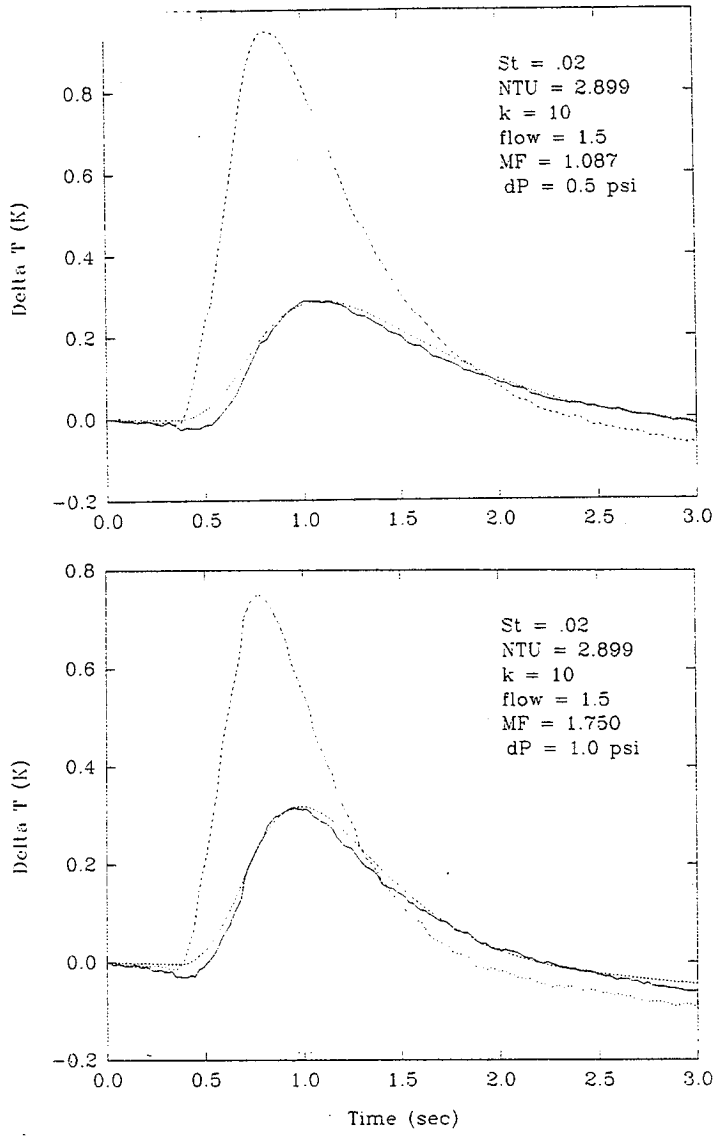

Fig. 32 Individual test runs of single blow rig showing input temperature pulse (dashed line) the measured output pulse (solid line) and the modeled output pulse (dotted line).

the pulse at the longer sample length. Since the model has by no means been thoroughly validated, mistakes or other approximations which cause major errors are possible.

The test apparatus may have problems as well. Flow around the sample exterior is one possibility. The samples were wrapped in carbon fiber sheet material to provide a reasonably snug fit between the sample exterior and the sample tube wall. In addition, the large expansion and contraction of the flow from the original 1" diameter pipe to a 1.75" diameter and back may be affecting the test results.

3.3.3 Thermal Conductivity

Thermal conductivity - A vacuum thermal conductivity apparatus was used to measure the axial thermal conductivity on three regenerator samples: slotted carbon-carbon, 200-mesh stacked screens, and 86% Brunswick stainless steel felt. To describe the thermal conductivity for porous media such as regenerators, the following form is assumed:

$$k_{eff} = \gamma f k_M$$

where k_M is the bulk thermal conductivity of the regenerator material, f is the volume fraction of the material in the regenerator, and the factor γ is a measure of the axial conduction effectiveness. For foil regenerators, one expects $\gamma = 1$; for an orthogonal array of wires, with 1/3 of the wires parallel to each of the three orthogonal directions, one expects $\gamma = 0.33$; for screens and felts, one expects a smaller value because the axial conduction paths are interrupted. In prior modeling of screens and felts, the value $\gamma = 0.3$ has been assumed.

The thermal conductivity apparatus has been constructed as illustrated in **Fig. 33**. The test procedure is to mount the sample, evacuate to pressure 1×10^{-5} Torr, and apply a constant power to the heated plate. The temperatures of the heated and cooled plates are monitored and within minutes steady state is achieved. The thermal conductivity, k, is calculated using

$$k = \frac{P\ L}{A\ \Delta T}$$

where L and A are the length and frontal area of the sample, respectively, ΔT is the steady state temperature difference, and P is the net power applied, corrected for a small leak rate determined with no sample mounted. **Table 12** shows the thermal conductivity for the samples tested. The carbon-carbon samples show that slotting for flow passages causes a drop in thermal conductivity, presumably because the 0.400" conductive carbon fibers are cut by 0.030" slots. The stainless steel screens show axial thermal conductivity 0.10 W/m-K which is less than 1% of the bulk stainless steel k-value, although the screen density is approximately 60%. The low k is presumably attributable to the poor contact between screens in this non-sintered sample. The LCP is an anisotropic liquid crystal polymer obtained from Hoechst-Celanese in the form of 2-mil film. It is reported to have a conduction anisotropy. The thermal conductivity was measured in three directions: through a stack of foils and in the two normal directions along the foil. The conductivity

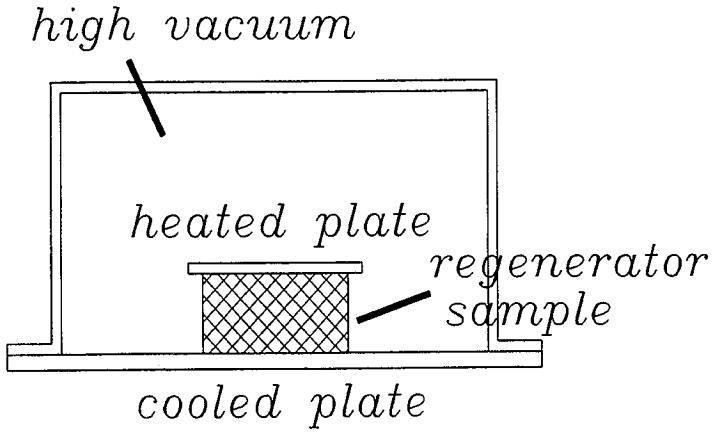

Fig. 33 Schematic for high vacuum thermal conductivity testing of regenerator samples.

through the stack of foils is observed to be $k < 0.01$ W/m-K, which is in a regime where the apparatus cannot resolve the value. The other two measurements were performed on scrolled samples in which the polymer orientation was circumferential or axial, prepared by cutting appropriate strips from the anisotropic polymer film.

Table 12 Observed thermal conductivity of selected regenerator samples.

Sample Material	Sample Size	Thermal Conductivity (W/m-K)
carbon-carbon	0.90" dia. × 0.50"	11.5 ±0.3
slotted carbon-carbon regenerator	1.0" dia. × 0.50"	8.4 ±0.3
SS screens	0.90" × 1" × 0.30"	0.10 ±0.01
LCP, through film	1" × 1" × 0.14"	0.00 ±0.01
LCP, circumfer.	0.50" dia. × 0.25"	0.00 ±0.01
LCP, axial	0.50" dia. × 0.25"	0.75 ±0.04

3.4 Small Engine Testing

Ross D-60 engine - Testing of composite regenerators was performed using a Ross Model D-60 Stirling engine lent to ESLI by General Pneumatics Corporation, Western Research Center (Phoenix, AZ) where it was built. The engine and regenerator space are shown in **Fig. 34**. This engine was used to gather performance (torque) *vs* frequency with different regenerators installed.

When the Ross engine was first installed and run with propane fuel, some vibration was observed, but it ran consistently enough to serve for 10-minute test durations. General Pneumatics engineers indicated that a bearing or crank failure might occur and this prototype engine could not be expected to survive hours of endurance testing. The engine had some minor difficulties during our testing when it failed to operate on a number of occasions. In one case debris from a nickel coating on the interior of the engine (or from carbonized oil) entered the snifter valve on the cold piston and ruined compression. In rebuilding the engine, it was necessary to iterate on seal clearance and piston heights to get satisfactory results. The seals have a tendency to swell when hot, which at first caused seizures with new seals, and they had to be trimmed for better performance.

A thermocouple was added to the hot head to allow temperature data to be monitored during operation. A flow meter for the propane tank was added to allow better control of the heat input. Attempts to use a cylindrical resistance heater achieved significantly less heating, presumably caused by poor heat transfer from the resistance coils to the engine hot head. To measure torque, a Magtrol magnetic hysteresis brake was installed on the engine output shaft.

Ross engine regenerators - Four metal test regenerators for the D-60 were fabricated from stainless steel 302 and nickel 200 solid foils:

1. 2 mil stainless/2 mil gap (50% porosity)
2. 3 mil stainless/3 mil gap (50% porosity)
3. 2 mil nickel/6 mil gap (76% porosity)
4. 2 mil stainless/6 mil gap (76% porosity)

A textile dimpling tool was used to set the foil spacing. One of these regenerators is shown in **Fig. 35.**

This suite of regenerators was selected to provide useful comparative data for comparison with modeling results. The original regenerator that came with the engine was a more loosely packed 2-mil steel foil with porosity closer to 70%. The nickel regenerator is included as an example of a high thermal conductivity material, otherwise identical to one of the stainless regenerators. This regenerator should have higher axial thermal conduction loss. Copper foil was not used because of excessive oxidation observed in air at 800°C.

Testing procedure - Test runs were performed as follows: the burner was run until the hot head temperature reached ~650°C and the engine was started with zero current applied to the hysteresis brake. The burner was fueled by a large ≥ 20 gal. propane tank which was pressure-

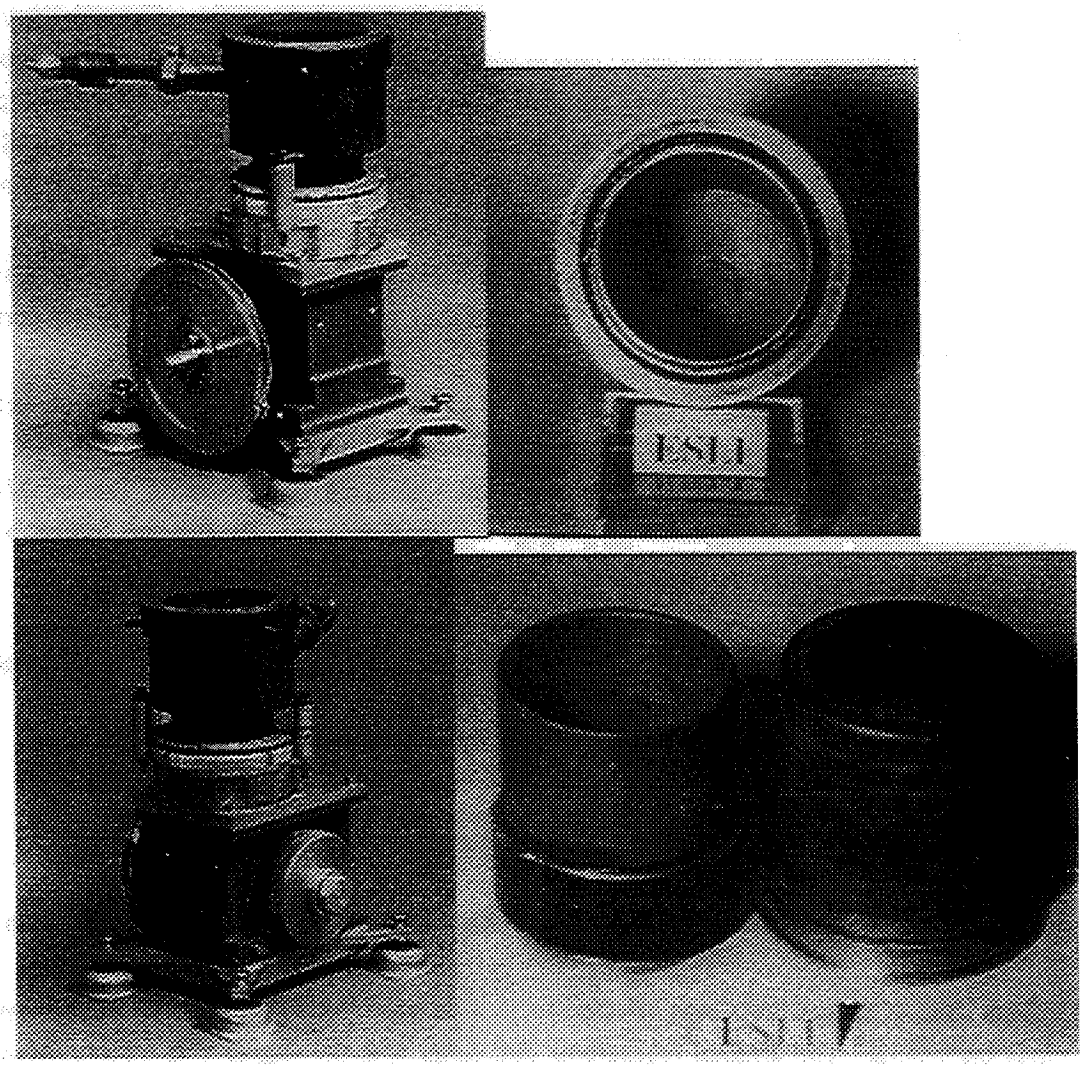

Fig. 34 Ross D-60 Stirling Engine (left) and annular regenerator space (right) whose outside diameter is 6.2 cm.

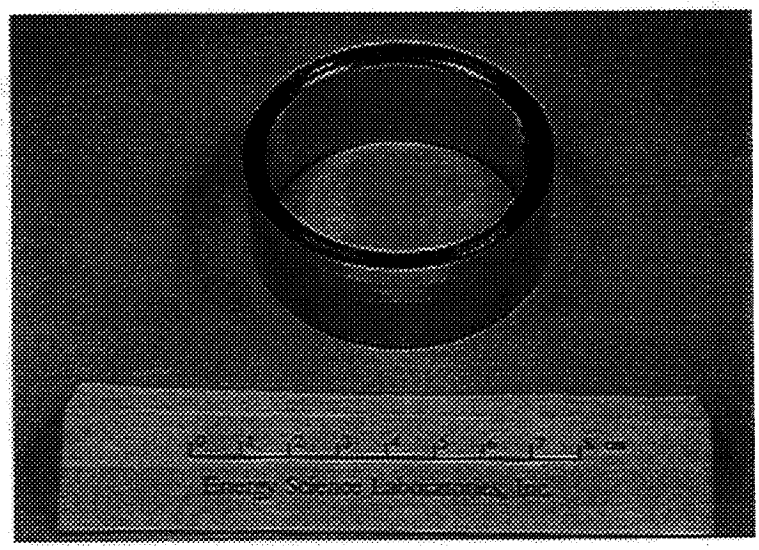

Fig. 35 Scrolled stainless steel regenerator for Ross D-60 Stirling engine (2-mil 304 stainless steel, 50% porosity).

regulated by a two-stage regulator. The temperature was controlled by regulating the regulator pressure manually. On typical runs the temperature could be maintained at 650±8°C. Torque was applied by a Magtrol Hysteresis brake and could be determined from a current vs. torque calibration curve. Torque could also be read directly from a dial push-pull force meter attached to a torque arm extending from the brake casing. Current to the brake was supplied by a Hewlett-Packard constant current power supply and was increased until the engine stalled. Engine speed was monitored by a magnetic pick-up and displayed on an LCD readout. Current and frequency reading were taken for each current setting. The temperature and flow of the cooling water were not monitored in the experiments but the flow was relatively constant between runs.

The original regenerator (1 mil SS; 88% porosity) was not long enough to completely fill the regenerator space in the engine, which introduced the possibility of shifting during and between runs. In the interest of reducing possible variability due to shifting, this regenerator was replaced with a tightly-packed regenerator (2 mil SS; 76% porosity), which had a similar expected performance from earlier modeling.

The original seals were retained throughout the runs. Replacement seals were oversized and tended to expand and seize in the cylinder while the engine was running. General Pneumatics had experienced this problem also, and said the new seals sometimes needed machining. However, proper jigging was not on hand, and the original seals were retained.

Engine reproducibility tests - **Fig. 36(a)** shows earlier tests of the original base regenerator (1 mil; 88% porosity), where performance was observed to decay over several runs. This was

(a)

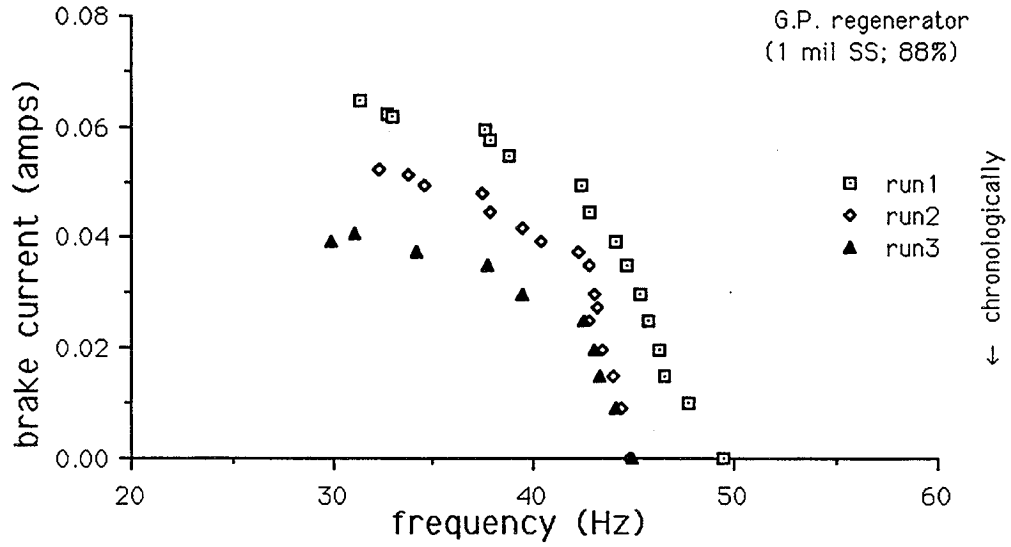

(b)

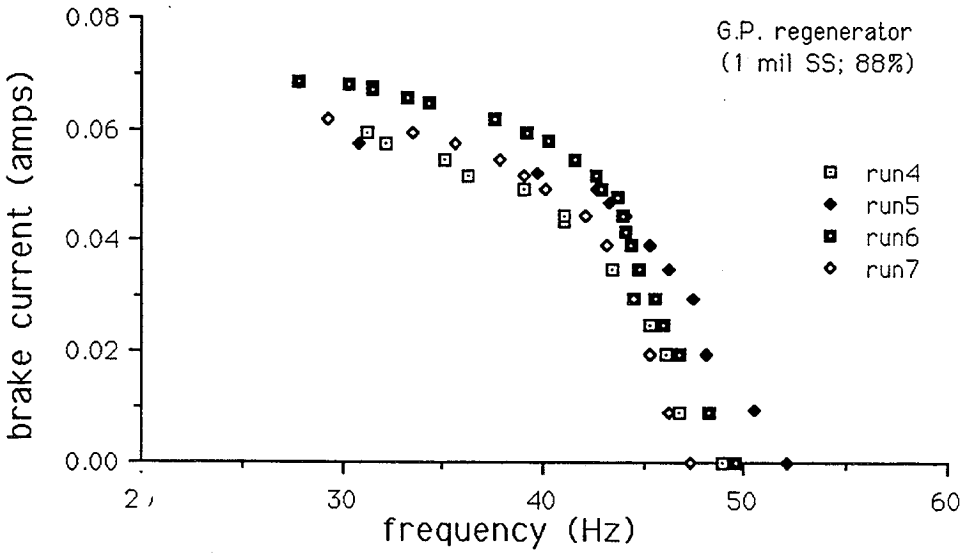

(c)

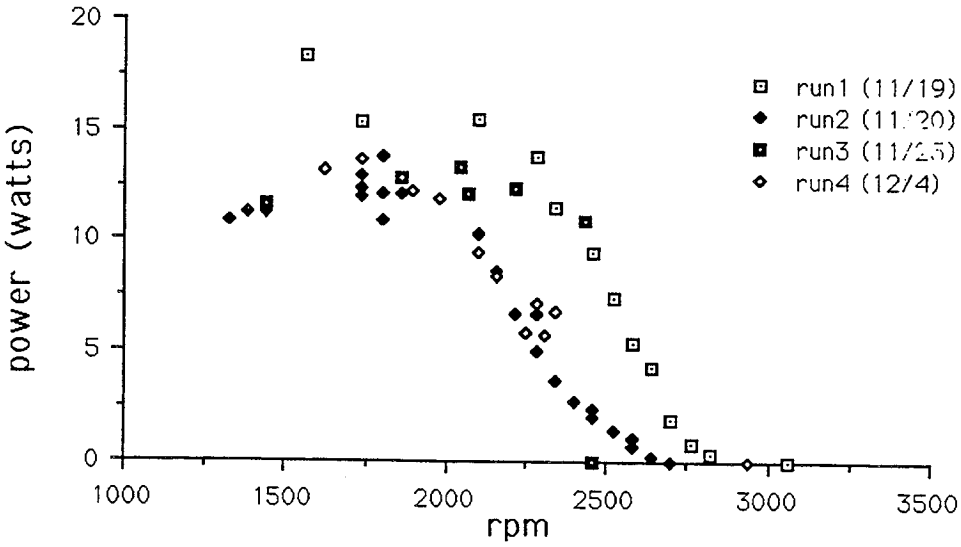

Fig. 36 Reproducibility testing of Ross engine.

thought to have been caused by fouling of the seals by two things: flaking of the nickel plating on the cylinder sleeve and contamination in the hot head during regenerator change-outs by solvents and skin oils. Subsequently, the hot head surfaces were wiped-down after handling without solvents, and the flaking nickel plating was sandblasted smooth which eliminated the problem of seal fouling.

Early reproducibility curves showed a band of different power curves which did not show a chronological decline over successive days, suggesting little or no wear of seals or mechanical parts (**Fig. 36(b)**). On another day of testing the reproducibility curves showed a similar band of curves with the same free-running engine speeds as the earlier tests (**Fig. 36(c)**). Again, the different power curves did not show a chronological decline in power. However, one interesting feature to note is what seems to be two different running modes at higher engine speeds, with better agreement between the curves at higher loading.

In earlier tests, the propane gas flow was held constant for each run, and this resulted in large hot head temperature variations during the run. The question was raised whether there was a strong coupling between shaft power output and hot head temperature in the range where the engine was operated. Hysteresis brakes can produce a steady torque over a broad frequency range, which allowed the power output curve to be traced out at two different torque settings. The engine power output was thus changed by adjusting the regulator pressure.

Fig. 37 shows a plot of the hot head temperature vs. frequency (which is directly proportional to power). Results show nearly constant power output over a temperature range between ~600°C and ~650°C at the two different torque settings. Following this test, subsequent runs were made at a fixed temperature of 650°C, compared to earlier runs which often exceeded 700°C. 650°C was chosen since it was within the constant torque range indicated by the test, and a lower running temperature was desirable since it reduced the chance of overheating the piston seals.

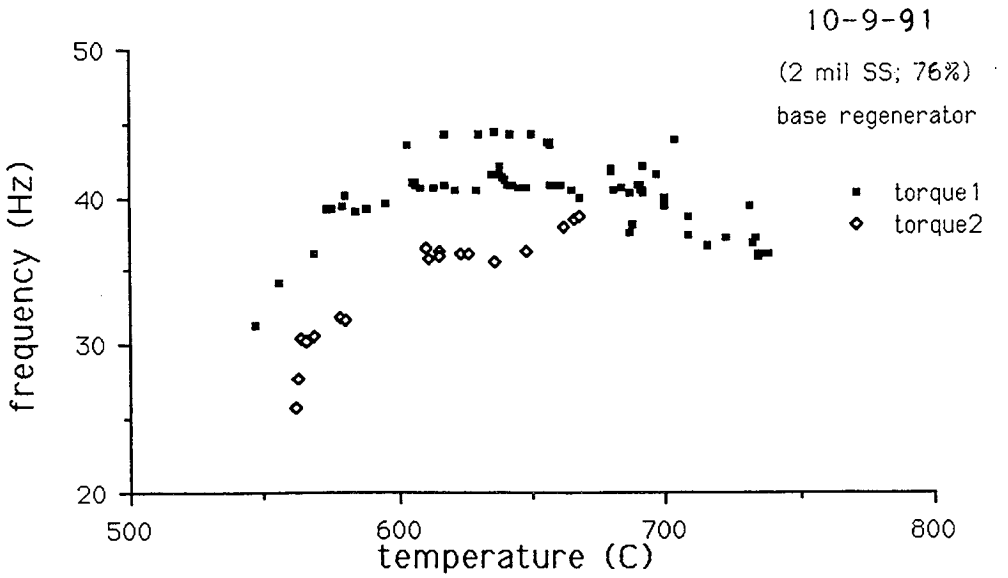

Fig. 37 Constant torque test of Ross engine frequency *vs* hot head temperature.

Metal foil regenerator comparisons - **Fig. 38** shows the results of early runs with the larger brake for four different regenerators. These runs were made at ambient pressure, but at higher temperatures (700°C ≤ T ≤ 730°C) than the later runs (642°C ≤ T ≤ 658°C). It is important to note that the relative ranking of the different regenerators is consistent with the ranking obtained by modeling with GLIMPS (see Fig. 31).

Later runs were made at different crankcase pressures. The engine was not fitted with a shaft seal, but the mechanical interface between shaft and bearing was close enough to allow low pressurization by flowing compressed air through the crankcase. This air flow through the crankcase carried away engine heat and made it difficult to control the temperature to 650°C. At a gauge pressure of 15 psi, this effect could be compensated for by an increased propane flow, but at 30 psi gauge this effect could not be adequately compensated for. In addition to this problem, differences in the crankcase pressure settings between runs became a significant source of error because the engine power was so strongly dependent on the crankcase pressure.

Fig. 39 show results of runs at three different pressures from four different regenerators. Although the curves overlap in spots, the main feature is that their relative ranking remains the same between pressure settings. The crankcase pressurization increased the overall power, but also tended to separate the four curves without affecting their ranking. It was thought that increasing engine power output might reduce the ratio of frictional losses to power output and allow better resolution between regenerators. At 15 psi resolution was improved between the 0.003" stainless steel, 50% porosity regenerator and the two 76% porosity regenerators. At 30 psi the heat losses and pressure setting differences between runs made the measurements more erratic and difficult to obtain.

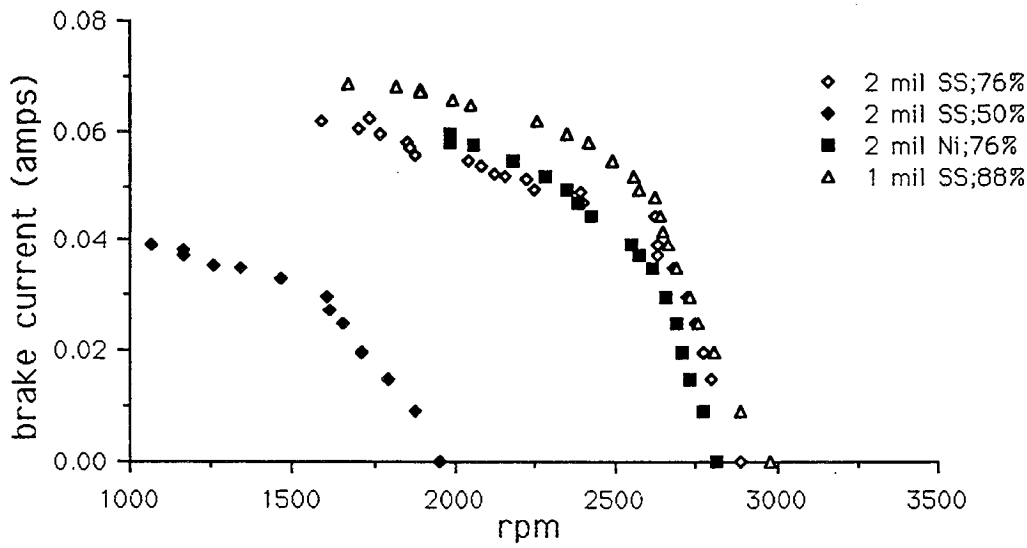

Fig. 38 Comparison of performance of foil regenerators in Ross engine.

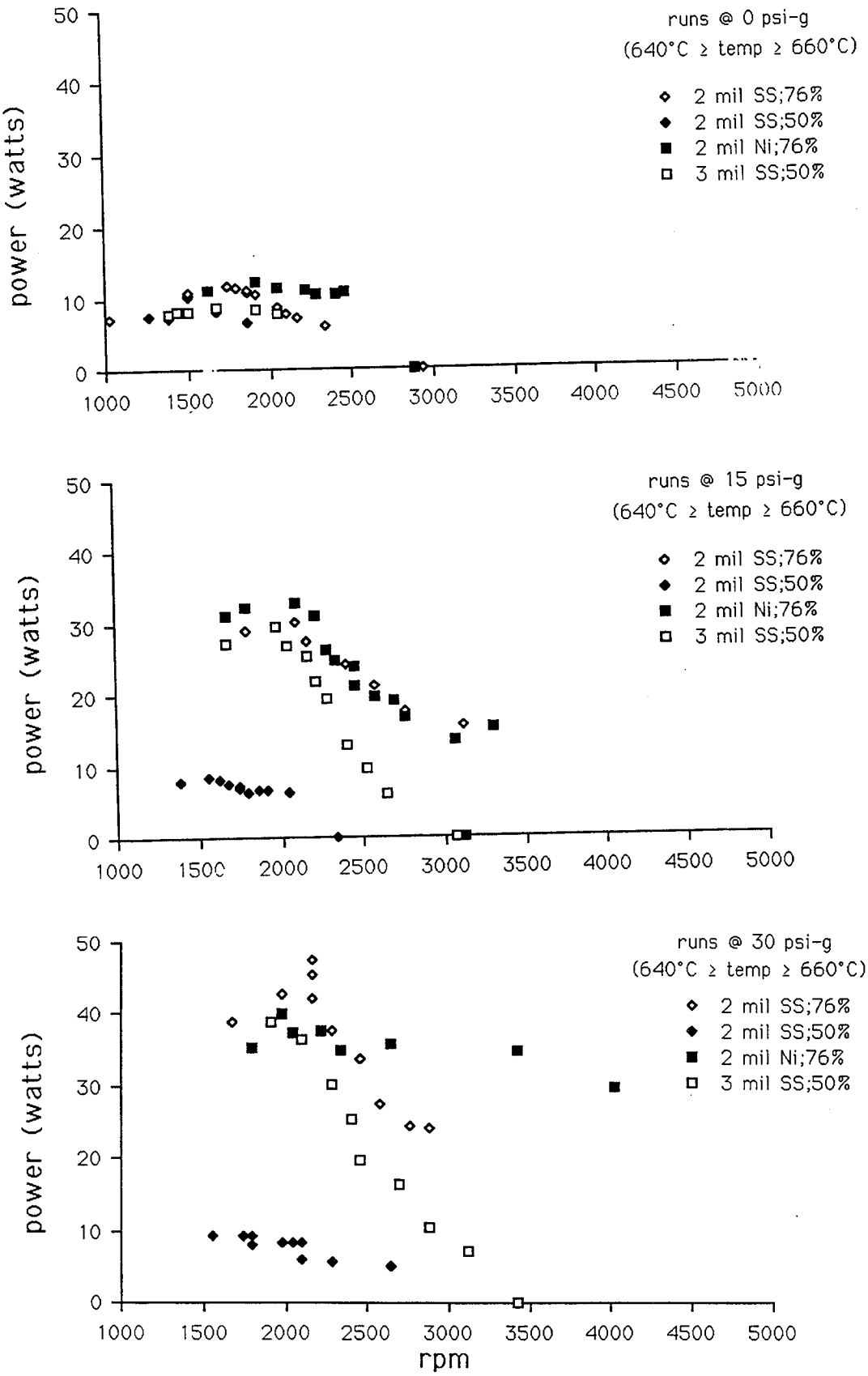

Fig. 39 Ross engine power *vs* pressurization for the foil regenerators.

Although the curves are more spread out, some of the points at peak output have multiple power values per frequency.

Differences in engine performance could be seen between the various regenerators. Porosity and foil thickness of the regenerators had a greater effect on engine performance than the regenerator material. Namely, differences between the 76% porosity Ni and SS regenerators could not be adequately resolved. Pressurizing the crankcase did somewhat improve resolution between regenerators, but a shaft seal is needed to prevent large variations in the performance due to heat loss and pressure variation. Relative ranking between the regenerators generally remained constant throughout the testing, although it is difficult to obtain a quantitative measure of these rankings. The Ross D-60 engine shows promise for exposing regenerators to working conditions inside the engine for survivability and endurance tests. Also, the relative simplicity of the engine makes it desirable since it can easily be taken completely apart and serviced should a regenerator break apart in the engine.

3.5 Prototype Regenerator Fabrication

The carbon vapor infiltration (CVI) process initially applies a thin layer of carbon on all surfaces bathed by the reactant gases at elevated temperature. Anisotropic carbon will normally deposit on each fiber or charred resin particle with the c-axis normal to the particle surface. Loose resin particles will be encapsulated and eventually tied together as the infiltration process continues. Similarly fibers are coated and joined to particles of char by the infiltrating carbon. Even when anisotropic carbon is deposited the macro effect of this process can be an isotropic interface composite due to the random orientation of connected porosity and cracks in the charred resin. The resulting interface structure will then be a composite with carbon fibers held to it by an interpenetrating layer of charred resin with randomly oriented anisotropic carbon infiltrated into it [Pierson, 1975].

Process variables influence the anisotropy of the deposited carbon and thus the properties of the fiber-carbon/carbon interface. The interface properties of this type of interpenetrating composite structure can also be dependent on the fiber precursor as well as the matrix structure. These materials have been shown to be superior to monolithic materials in their resistance to brittle failure and coefficient of thermal expansion (CTE) mismatch tolerance. Where large CTE mismatches exist, improvements in both mechanical properties and thermal conductivity have been achieved by a graded interface approach.

Initial CVI coatings - The carbon vapor infiltration process was tested on a scrolled carbon fiber felt structure having diameter 1 cm and length 5 cm. Carbon vapor infiltration was performed at 1180°C with 10 Torr propylene for 3 hr. This results in an anisotropic carbon coating of thickness 3 μm and the increase in strength is readily apparent to the touch. The 25 mm high scroll was loaded with a 200 g weight; the uncoated felt crushed by 1.5 mm and the coated felt crushed only 1.0 mm.

A flocked Dylan plate was prepared with flocked 2.5 mm long P-120 fibers embedded approx. 0.3 mm into the Dylan and treated with the above CVI process. The channel dimensions were 2 mm wide, 12 mm long and 10 mm high. After coating the channel was inspected and non-uniformities in the coating were observed throughout. Also at the upstream end the coating was thicker than at the downstream end.

Reduced pressure CVI - To improve the coating process the reactor pressure was reduced to 10 kPa from the atmospheric pressure conditions (100 kPa). This required installing a cold trap, a roughing pump, a pressure gauge and control valves. The benefits of reducing the pressure in the carbon vapor infiltration process are

- higher reactant drift velocity
- longer diffusion distance, longer mean free path
- longer region of good deposition in the reactor
- less homogeneous gas-phase reaction products affecting microstructure
- less convection
- greater penetration of uniform coatings in porous substrates

The penalty is that deposition occurs more slowly and longer deposition times are required.

HP-1000 regenerators - Carbon regenerator preforms were fabricated by electroflocking P-120 carbon fibers to a mandrel made of laminated Grafoil bonded with phenolic resin and carbonized. The dimensions are given in **Fig. 40**. CVI was performed at 1130°C using hydrogen-diluted propylene (30% H_2, 70% C_3H_6) feed gas at 200 cm^3/min and pressure 2 Torr for approximately 80

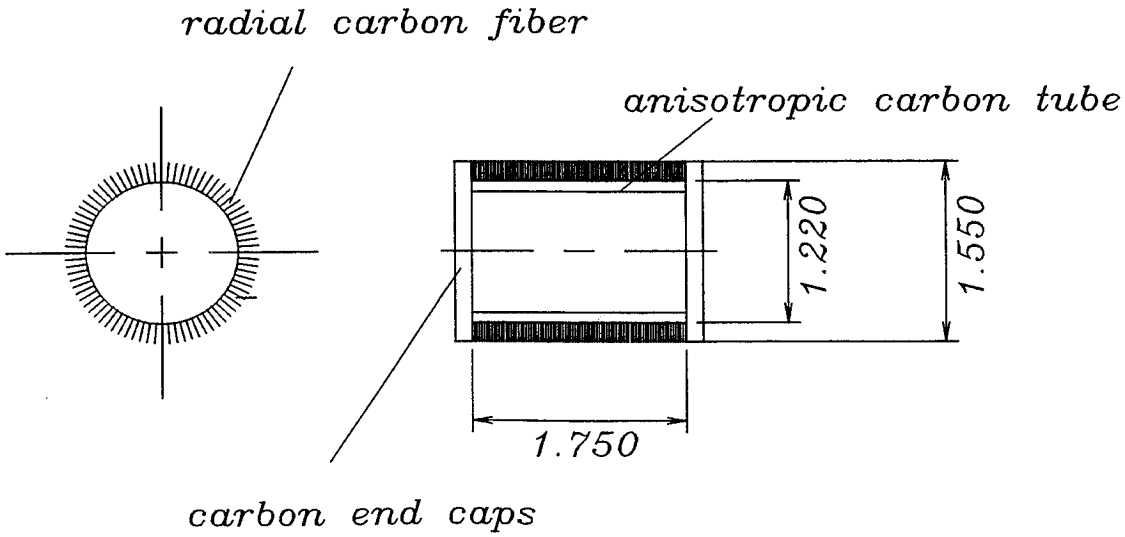

Fig. 40 Dimensions of Prototype HP-1000 regenerator (in inches).

hours. The processing was interrupted a number of times to check on the fiber diameter, where the goal was to achieve a fiber diameter of 80 μm.

The appearance of the prototype regenerator product is shown in **Fig. 41** and **Fig. 42**. Three prototype regenerators were fabricated and delivered to NASA Lewis Research Center. A specimen of this type of regenerator was used in single-blow rig testing (Section 3.3.2), and a similarly prepared specimen, but with other dimensions, was fabricated for endurance testing in the Ross engine (Section 3.4).

Ross engine regenerator testing - A flocked carbon regenerator ("graphite") equivalent to the prototype regenerator was tested in the Ross D-60 engine. The observed performance is shown in **Fig. 43**. The standard stainless steel regenerators were also run under equivalent conditions of the seals for comparison purposes. It may be observed that the engine performed best with the graphite regenerator. It was run for a total of 21 min 48 sec in dry nitrogen. The mass of the regenerator changed from 163.55 g initial to 163.31 g final, showing essentially no mass loss. Inspection of the regenerator following the test showed no noticeable debris or deformation of the regenerator.

4 CONCLUSIONS

4.1 Composite Regenerator Characteristics

The original CMR design in which fine fibers cross a flow channel and embed in the channel wall was not accomplished because of fabrication difficulties in the various configurations tested. It was demonstrated that suitable fiber geometries could be established with electroflocking and that the fibers would survive the dynamic pressure in the engine, but the challenge remains to embed the flock in a suitable precision net shape channel wall.

Prototype carbon regenerators with a thick radial carbon fiber feature have been successfully fabricated by electroflocking and CVI. Such regenerators have been tested in a blow rig and in a small Stirling engine where the regenerator not only survived limited endurance testing but the relative thermal performance was the best of the various regenerators tested in the engine under equivalent conditions. However, the single-blow rig tests indicated poor performance with the carbon regenerator, and it is not clear whether this is a true representation of the design or was caused by test errors.

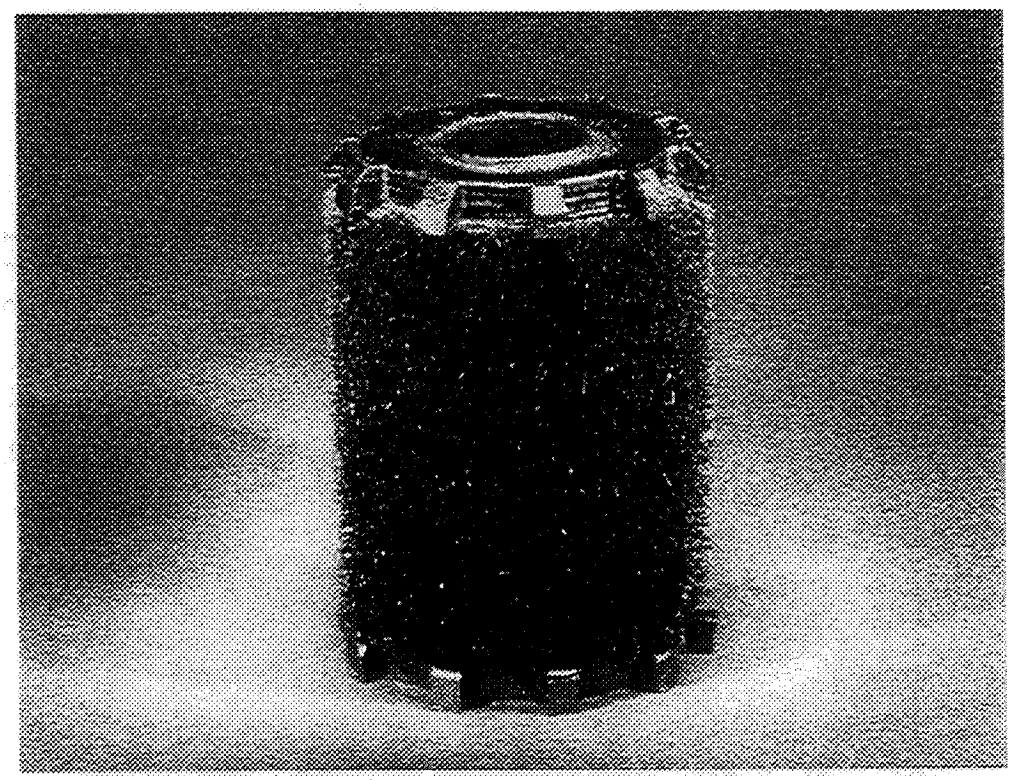

Fig. 41 Prototype HP-1000 carbon regenerator.

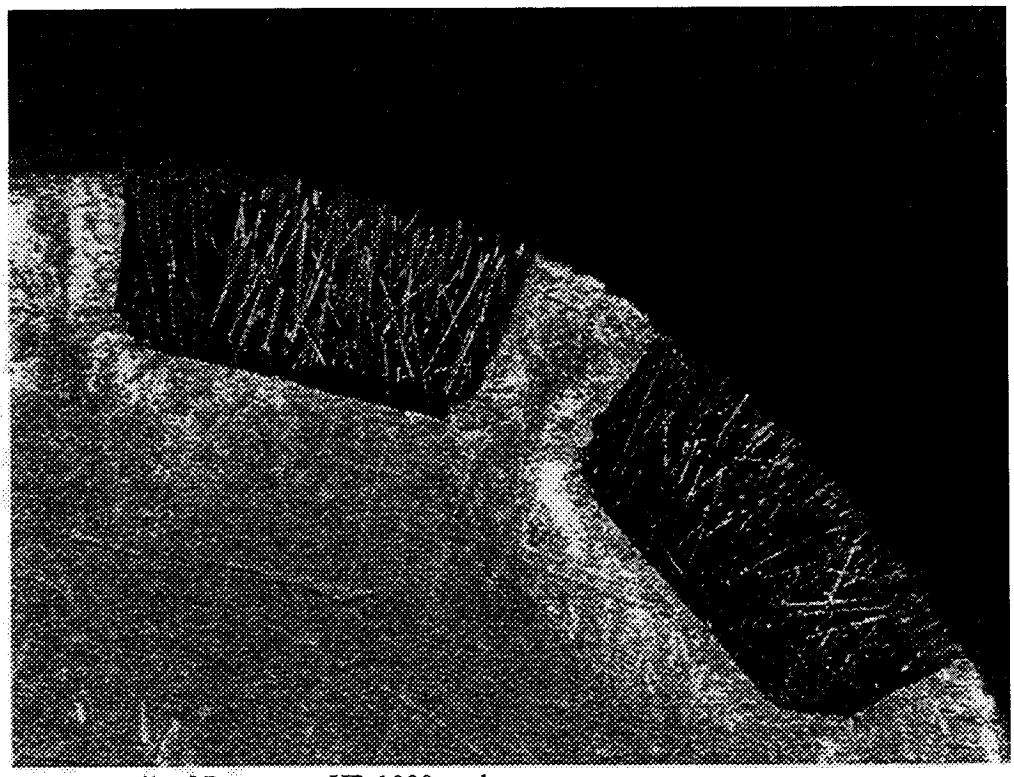

Fig. 42 Detail of Prototype HP-1000 carbon regenerator.

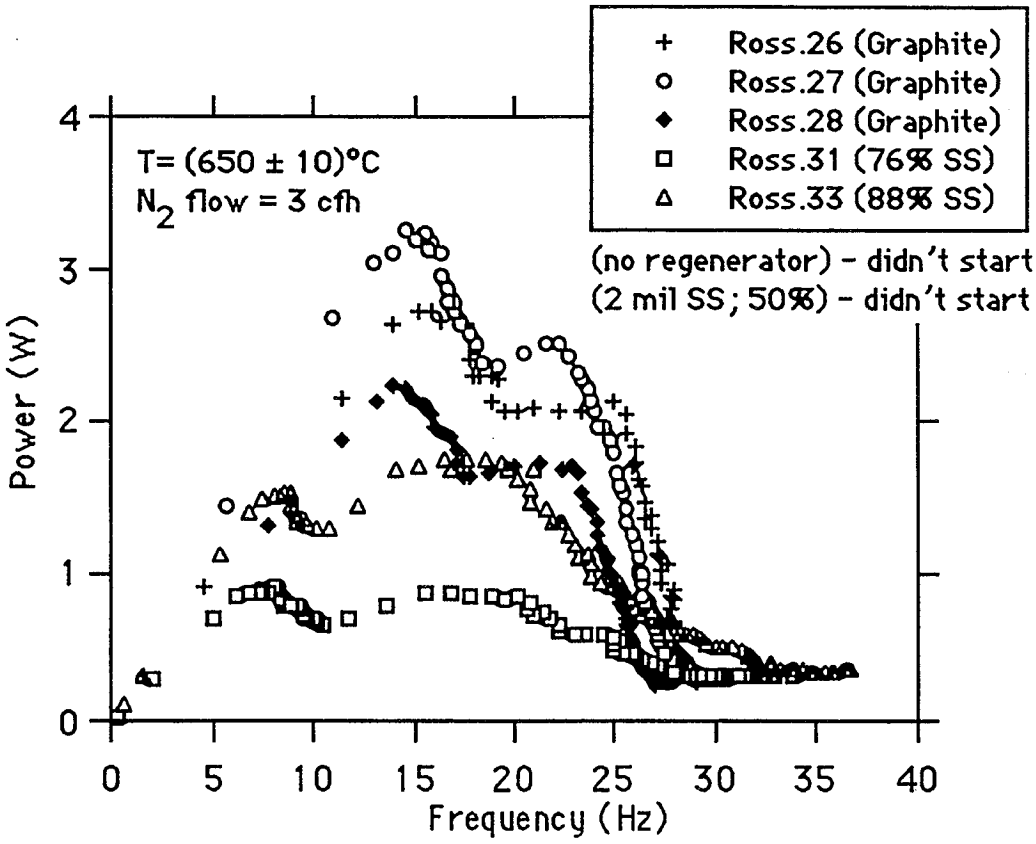

Fig. 43 Comparative Ross engine regenerator testing.

4.2 Applications

The ability to orient transversely a large array of fine carbon pin fins by electroflocking and CVI is the leading achievement of this effort. There are regenerator applications in engines as well as cryocoolers. Especially for cryocoolers operating below 10 K there is potential benefit in using composite matrix design with high-*c* materials in the walls. The fiber architecture may be useful in other heat exchanger applications where extended surface effects are required, particularly gas-side heat exchangers. The 1-D flocked fiber architecture may also be useful for composites requiring high through-thickness conductivity or transverse reinforcements.

References

Amon, C. H. and Mikic B. B., Numerical Prediction of Convective Heat transfer in Self-sustained Oscillatory Flows," J. Thermophysics, V. 4, pp. 239-246, 1990.

Burkhardt, W.M., et. al., Formed platelet liner concept for regeneratively cooled chambers, AIAA Paper 90-2117

Cook, J.L., Lambdin, F., "Fabrication of Carbon-Carbon Composites Using Electrostatic Fiber Deposition," SAMPE Quarterly, Vol. 2, (1971) pp. 38-47.

Foster, B. and Patton, J. eds., *Advances in Ceramics--Ceramics in Heat Exchangers*, American Ceramic Society, Inc, 1985

Fucinari, C. A., Regenerator matrix physical property data, NASA-CR-159854, 1980.

Hutchison R. A., Heat engine regenerators: research status and needs, DOE Report PNL-6278, 1987.

Jones, J. D., Performance of a stirling engine regenerator having finite mass, J. of Engineering for Gas Turbines and Power, ASME Transactions 108, 1986, pp 669-673.

Kane, J.L., "Orientation of Small Diameter Discontinuous Reinforcements for Structural Composites," NTIS Technical Report No. AFML-TR-69-288, Nov 69, 110p

Kays, W.M. and London, A.L., *Compact Heat Exchangers*, McGraw-Hill, Third Edition, 1984.

Knowles, T. R., "Metal/Phase-Change Material Composite Thermal Storage Materials," AIAA Paper-87-1489, June, 1987.

Miyabe, H., et. al., Approach to the design of Stirling engine regenerator matrix using packs of wire gauzes, 17th IECEC 829306, 1982, pp. 1839-1844.

Pierson, H.O. and Lieberman, M. L., Carbon **13** (1975) pp. 159-166,

Pucci, P. F. et al., Single-blow transient testing technique for compact heat exchanger surfaces, Journal of Engineering for Power, January 1967, pp. 29-40.

Radebaugh, R., and Louie, B., A Simple, First Step to the Optimization of Regenerator Geometry, Third Cryocooler Conference, Boulder, CO, 1984.

Simetkosky, M. A. et al., Development, analysis, and testing background of the MOD II automotive Stirling engine., Proceedings of the 3rd International Stirling Engine Conference, Rome, Italy 1986 Jun 25-27, p 129-146, 1986.

Slaby, J. G., Free-piston Stirling technology for space power, NASA Lewis Research Center, IAF-ICOSP89-5-7, February, 1989.

Sullivan, T. J., NASA Lewis Stirling Engine Computer Code Evaluation; NASA CR-182248, 1989.

Takahashi, S., et al., On the flow friction and heat transfer of the foamed metals as the regenerator matrix, 2nd International Conference on Stirling Engines; Shanghai, China; Jun 21-24, 1984.

Tew, Roy C. Jr.; Status of several Stirling loss characterization efforts and their significance for Stirling space power development.; 1988 IECEC Jul 31-Aug 5 ,pp. 113-119, 1988.

Thonger, J. C. T. and Rice, G., Regenerator effectiveness and fluid friction measurements, 3rd International Stirling Engine Conference, Rome, Italy, Jun 25-27, 1986 (Assoc Termotecnica Italiana) pp. 335-349.

Walker, G., *Stirling Engines*, Claredon Press, Oxford, 1980

Walker G. and Vasishta, V.; Heat-transfer and flow-friction characteristics of dense-mesh wire-screen Stirling-cycle regenerators; Advances in Cryogenic Engineering 16, 1971, pp. 324-332

Zukauskas, A.; Heat transfer from tubes in crossflow, Advances in Heat Transfer, 8, Harnett, J.P. and Irvine, T.F., Jr., eds., Academic Press, 1972, pp. 93-160.

Appendix A

27th IECEC (San Diego, CA, 8/3-7/92)
Abstract/Paper 92IEC355
Session Code: SC01 (John Corey)

PULSED SINGLE-BLOW REGENERATOR TESTING

Authors:

1. J. C. Oldson Energy Science Laboratories, Inc., 6888 Nancy Ridge Drive, San Diego, CA 92121-2232
2. T. R. Knowles Energy Science Laboratories, Inc., 6888 Nancy Ridge Drive, San Diego, CA 92121-2232
3. J. Rauch Sverdrup Technology, 2001 Aerospace Parkway, MS-SVR, Cleveland OH 44124

ABSTRACT

A pulsed single-blow method has been developed for testing of Stirling regenerator materials performance. The method uses a tubular flow arrangement with a steady gas flow passing through a regenerator matrix sample that packs the flow channel for a short distance. A wire grid heater spanning the gas flow channel is used to heat a plug of gas by approximately 2 K for approximately 350 ms. Foil thermocouples monitor the gas temperature entering and leaving the sample. Data analysis based on a 1-D incompressible-flow thermal model allows the extraction of Stanton number. A figure of merit involving heat transfer and pressure drop is used to present results for steel screens and steel felt. The observations show a lower figure of merit for the materials tested than is expected based on correlations obtained by other methods.

INTRODUCTION

The regenerators of Stirling cycle machinery are very compact heat exchangers whose performance critically influences machine efficiency. High machine efficiency requires regenerators with high thermal effectiveness and low pressure drop. Novel composite matrix regenerator structures are becoming available that may enable higher performance than conventional regenerator materials, and it is desired to have a simple means of screening the performance characteristics of regenerator materials.

Single-blow methods have been used [1,2,3] to measure the heat transfer coefficient. In prior work a constant velocity gas flow passes through the sample, and a step change in gas temperature upstream from the sample is imposed by switching to a gas flow of different temperature. The gas temperature immediately downstream from the regenerator sample reveals the heat transfer coefficient and thermal effectiveness of the regenerator. The maximum slope of the temperature rise is used to obtain the heat transfer characteristics.

PULSED SINGLE-BLOW RIG

The pulsed single-blow rig is another means of measuring thermal effectiveness in small regenerator samples which allows greater control over input gas temperatures. When coupled with numerical modeling that simulates the response of the sample for the entire pulse, both the temperature rise and decay, it is expected that more accurate and detailed information on regenerator performance will be obtained.

REYNOLDS NUMBERS - The rig is designed for use at ambient pressure and temperature. The Reynolds numbers in the test sample and the Stirling engine regenerator should be equal to permit scaling between the two cases. Because the same material is used in both cases, the characteristic length in the Reynolds number is unchanged, and we need only to equal the flow velocity divided by kinematic viscosity in the two cases. For the engine, helium is the working fluid at an average temperature of 500 K and an average pressure of 10 Mpa, and the kinematic viscosity is 2.984×10^{-6} m^2/s [4]. For the rig which uses nitrogen, the kinematic viscosity at 20°C and 1 atmosphere is 15.05×10^{-6} m^2/s [5]. For equal Reynolds numbers between the two cases, the nitrogen flow velocity in the test rig must be approximately five times higher than the helium flow velocity in the engine.

The gas flow velocities in engines depend on the displacer/piston frequency, stroke, as well as the ratio between displacer/piston area and regenerator frontal area. Typical values are: frequency = 60 Hz, stroke = 1.5 cm, area ratio = 0.7, so that the average flow velocity is approximately 2.5 m/s. The phase angle is ignored and the average gas flow velocity is taken as the peak displacer/piston velocity. Because of the higher peak velocity and the higher Reynolds number at

the cold end of the engine, we take 5 m/s as a measure of the maximum gas flow velocity in the engine, and therefore require a corresponding maximum nitrogen flow velocity of 25 m/s is required in the test rig.

EXPERIMENTAL ARRANGEMENT - The test rig consists of heater, manometer ports, thermometers, and regenerator components modularized in clear polycarbonate tube sections having 25 mm inside diameter. The regenerator test samples are mounted in tube sections having 18 mm inside diameter.

The setup currently uses a compressed nitrogen cylinder to supply the gas flow, regulated at 0.8 MPa as the gas enters the test apparatus. A flow meter capable of 500 L/min (standard liters per minute) is used to monitor the flow, corresponding to a flow velocity of 32 m/s through a 0.75 diameter tube at ambient conditions.

Pressure drop is measured using a Validyne PS309 Digital Pressure Manometer operated in the differential pressure mode. It has a full-scale differential pressure range of 8 psi and an accuracy of 0.02 psi. Mass flow is measured using a Teledyne Hastings-Raydist HMF-201 that has a full-scale range of 500 L/min and an accuracy of 5%. Readings from the flow instruments are recorded manually.

The temperature pulse is provided by a fine copper wire heater supported by a plastic frame with a 25-mm hole in the center. The wires are spaced by slots in the edge of the frame, made by pressing a hot 8-32 bolt partially into the plastic. The average spacing is about 2 wires per millimeter. A second heater section is mounted at right angles to the first, to provide more heating to the gas flow. The power for the heat pulse is supplied by two 12 V batteries connected in series, with the pulse duration controlled by computer. The heater resistance is 9.0 Ω, so that the current is 2.67 A and the power is 64 W. Approximately half the power appears in the gas, and the remainder is dissipated in the portions of the wire embedded in the frame. This heat is dissipated slowly by conduction to the ambient and is presumed to not affect the experiment.

The gas temperature is measured upstream and downstream from the regenerator test sample. Both sensors use Type K thin film thermocouples, 12 μm thick, and mounted on 75 μm polyimide film (#20112 from RDF Corp.). The thermocouples are mounted broadside to the flow (polyimide film facing downstream).

The voltage output from the thermocouples is amplified by two Analog Devices AD524CD Precision Instrumentation Amplifiers, operating at a gain of 1000. A low pass RC filter with a cut-off frequency of about 10 kHz is added to each output to reduce high frequency noise coming from the computer. This filter leaves intact the signal as well as the other large noise source at 60 Hz.

The amplified signals are passed to an Industrial Computer Source AIO8PGA analog to digital computer board, mounted in a personal computer. The board is configured to digitize the differential input voltage on the two input channels, with a sampling rate of about 240 Hz on each channel. Each digitized voltage is then stored in memory. Following a typical data run of 10 seconds, the data for each channel is processed by averaging 4 sequential points to eliminate most of the 60 Hz noise, and then converting the voltage to temperature. A screen plot of the two temperatures vs. time is then displayed to insure a good set of data was obtained.

The AIO8PGA board is also used to control the heater pulse length, and therefore the total energy of the pulse. One of the digital input/output lines is driven high for a fixed time interval of approximately 350 milliseconds. This line controls the heater through an NPN Darlington transistor used as a solid state switch.

MODELING

The rig flow geometry is one-dimensional (1-D) and the temperature changes induced by the thermal pulse are small, on the order of 2 K and therefore less than 1% of absolute temperature. The model used to describe the thermal behavior of gas interacting with the regenerator matrix is based on the following assumptions:

- 1-D temperature distribution
- incompressible flow
- constant flow velocity
- constant thermal properties
- finite axial matrix conductivity

The partial differential equations describing this model, which have been investigated by Schumann [6], Creswick [7], Pucci et al [1], and others, are:

$$\frac{\partial T_s}{\partial t} = \alpha \frac{\partial^2 T_s}{\partial^2 x} + \frac{b\, h_c}{\rho_s\, c_s\, A_s} (T_g - T_s) \qquad (9)$$

$$\frac{\partial T_g}{\partial t} = \frac{b\, h_c}{G\, c_g} (T_s - T_g) \qquad (10)$$

The non-dimensional form is:

$$\frac{\partial T_s}{\partial \tau} = \lambda\, NTU \frac{\partial^2 T_s}{\partial^2 z} + (T_g - T_s) \qquad (11)$$

$$\frac{\partial T_g}{\partial z} = (T_s - T_g) \qquad (12)$$

A program to solve these equations has been written and compiled in Microsoft FORTRAN 5.1. Running on a 33 MHz 486 personal computer, the program executes in 10 minutes for a 100-node case that simulates approximately 7 seconds of experimental time and is sufficient for samples with a total $NTU < 50$. For larger NTU more nodes must be added to assure that heat transfer to each node is small enough for convergence.

The current approach is to simulate the complete temperature pulse response of the gas passing through the regenerator and we manually fit the various features of the pulse shape, including the delay, the rise, the maximum height and the decay. This approach differs from prior work that fits the initial rise of a step function. Schumann [6] derives an analytic solution for a special case without matrix heat conduction and with a step function change in temperature starting from equilibrium. Differentiation yields the maximum slope of the solution, and that form is used by Pucci [2] for data reduction. Our rig has not been used in a step-function mode, because our heater can only be used for short pulses, we cannot at present assess the difference between the two approaches. However it seems that attention to only the initial temperature rise for data reduction is inherently less accurate.

The effect of increasing *NTU* in the case where the solid thermal conductivity equals zero was investigated. For $NTU << 1$, the input pulse experiences an attenuation of amplitude as a small amount of the heat is removed from the gas stream and reintroduced a short time later. For $NTU >> 1$, the outgoing pulse is a delayed version of the input pulse. As *NTU* increases, it therefore becomes harder to extract the heat transfer coefficient, because the pulse shape is asymptotically approaching the input pulse shape.

MODEL FITTING PROCEDURE - The procedure for extracting parameters from the data involves manual curve fitting at present. First, the flow parameter Wc_g (J/K-s) is matched by adjusting the location in time of the measured downstream gas temperature with the modeled output. This procedure has been fairly simple in those cases analyzed to date. The reason for the discrepancy between the nominal and measured flow parameter has not been found. In most cases, it is higher than the nominal error on the flow velocity itself. Errors in the specific heat of the solid contribute directly to the flow parameter, so these may be part of the source. Measured values for the thermal conductivity are used in modeling. The problem then reduces to a single variable fit between the experimental and model output. Although we have fitted the curves manually based on visual agreement, this procedure should be replaced with an algorithm that minimizes some measure of the error between observed and simulated temperature curves.

If thermal conductivity data is not available and the sample response is substantially modified by the thermal diffusion, then the data is harder to interpret. Increasing the thermal conductivity has a very similar effect to decreasing the heat transfer coefficient, thus extracting both thermal conductivity and the convective heat transfer coefficient is ambiguous.

TEST RESULTS

PULSED SINGLE BLOW MEASUREMENTS - Test data for two conventional types of regenerator materials are reported here, together with the simulated output temperatures calculated according to the above model. Figure 1 shows data and simulation for steel felt (Brunswick feltmetal, provided by NASA Lewis Research Center) having 25-micron wire diameter. The steel felt has a porosity of 0.84. The sample length is 0.64 cm. Figure 2 shows data and simulation for market grade, 200 mesh (M200) stacked steel screens having 53.5-micron wire diameter. The stainless steel screens were not sintered, but they were bonded at the edge with Teflon to hold the 1-cm stack together. The screens have a porosity of 0.67.

The simulation curves show very good visual agreement with the observed output temperatures, and differ only by a slight drift in the temperature data attributable to a small gas cooling trend (due to expansion from the high pressure source) not accounted for in the model.

THERMAL CONDUCTIVITY - A separate experimental setup was developed to measure the vacuum thermal conductivity of the samples. A simple method involving one heater and two thermometers was used to measure the temperature drop over a known distance with a known heat flux. The observed axial thermal conductivities are k = 0.24 W/m-K for the steel felt, and k = 0.30 W/m-K for the M200 steel screens.

FIGURE OF MERIT - The results of model fitting are shown in Table I for the two screen and felt samples. The data may also be presented in terms of a figure of merit defined as the ratio of the Colburn *j*-factor ($St \times Pr^{2/3}$) divided by the Fanning friction factor, *f*. These data and are shown graphically in Figure 3 together with expectations based on correlations from Radebaugh and Louie [8] which are based on Kays and London data. Our results differ from those correlations in that the observed figures of merit are significantly lower. Our pressure drop measurements are consistent with the results reported by Koester et al. [9] for steady-state flow measurements on steel felt having 13-micron wire

Table 1 Heat transfer and pressure drop data.

Sample	Reynolds	Fanning	Stanton
M200	41.6	1.82	0.20
M200	71.7	1.16	0.12
M200	98.2	0.87	0.10
felt	17.8	5.03	0.20
felt	30.6	3.34	0.15
felt	51.7	2.26	0.10
felt	85.8	1.55	0.09

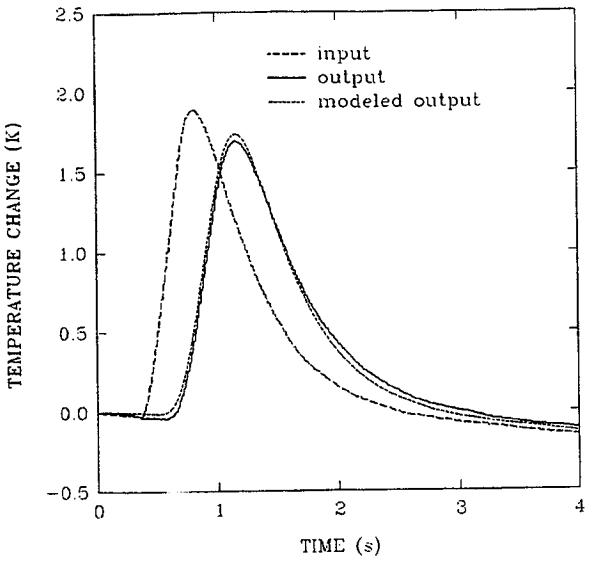

Figure 1 Temperature data for steel felt at external flow velocity of 9.09 m/s.

diameter. The felt has lower performance than the stacked screens, both because it has lower Stanton numbers and because it has significantly higher pressure drop, perhaps resulting from less ordered crossflow elements than in the screen material.

ERROR ESTIMATES - A sensitivity analysis for most of the data points has been performed, to set a bound on the magnitude of error caused by an inability to distinguish similar Stanton numbers. The errors are lowest for the two highest flow rates for both samples. For the two highest flow screen data, the error is estimated as about 10%. For the lowest flow rate screen data, the value of 0.2 for the Stanton number has an estimated range from 0.15 to 0.3. For the steel felt samples, the two highest flow rate data points have an estimated error of 10%. The range on the second lowest flow rate data point, St = 0.15, is estimated between 0.12 and 0.18, while the lowest flow rate St = 0.20 has an estimated range between 0.15 and 0.3. The larger uncertainty on the high side is due to the increasing insensitivity to changes in the Stanton number.

The pressure drop errors have not been estimated for the screens, but should be less than the 10% error in the Stanton number for all flow rates. The pressure drop error for the steel felt is assumed to be at most 20% too low.

RECOMMENDATIONS

Some changes in the test setup and method of analysis that may give improved results are: (1) The compressed gas supply can be replaced with a lower pressure compressor or vacuum pump. Aside from convenience, the main benefit is the reduction of the gas cooling resulting from expansion out of the high pressure tank. (2) The present heater could be improved by

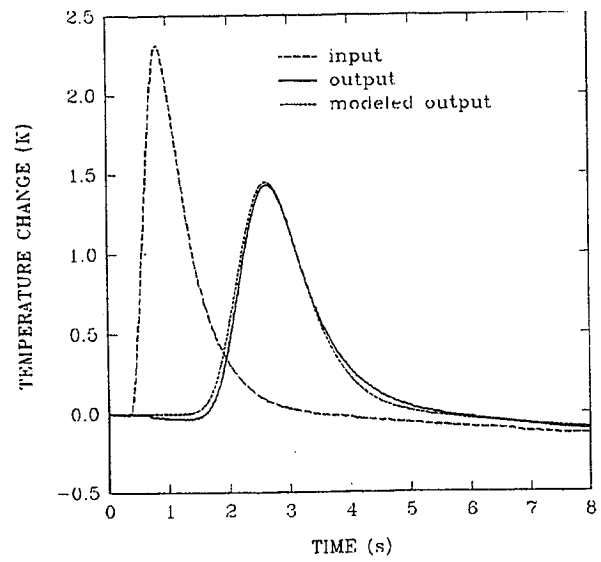

Figure 2 Temperature data for stacked screens M-200 at external flow velocity of 6.69 m/s.

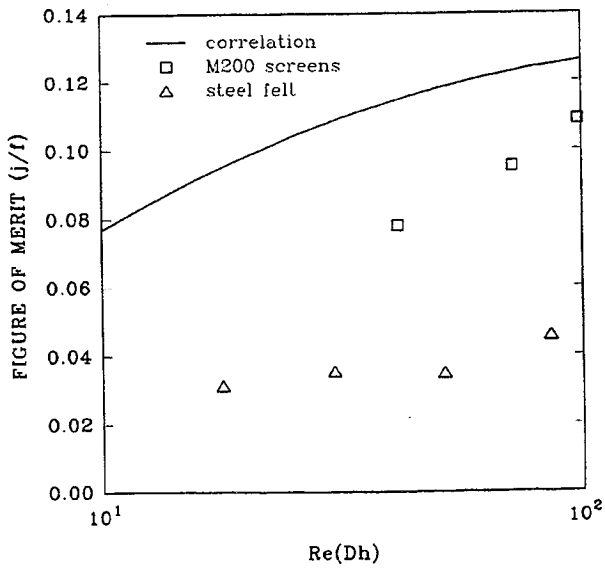

Figure 3 Figure of merit (j/f) for steel screen and felt regenerator samples, and Radebaugh correlation [7].

an even finer heater that has no parts embedded in resistive materials, to allow faster pulsing as well as step functions, sinusoidal variations, etc. (3) The spacing between the various elements in the test rig should be reduced to cut down on heat loss and maintain a more uniform velocity across the flow area. (4) An algorithm to automatically extract quantitative fitting parameters would be preferable, to reduce subjectivity in the fitting and to potentially reduce the time required to perform the fitting.

NOMENCLATURE

A_s	solid cross-section area for heat conduction (m^2)
b	wetted flow perimeter (m)
c	specific heat at constant pressure (J/kg-K)
D_h	hydraulic diameter (m)
f	Fanning friction factor
G	gas mass flow rate (kg/s)
h_c	heat transfer coefficient (W/m^2-K)
j	Colburn j-factor
k	solid thermal conductivity (W/m-K)
L	total sample length (m)
NTU	number of heat transfer units = 4 *St* L/D_h
Pr	Prandtl number
Re	Reynolds number
St	Stanton number
T	temperature (K)
t	time (s)
x	distance along sample (m)
z	dimensionless length variable = N_{TU} * x/L
α	solid thermal diffusivity (m^2/s)
λ	kA_s / Gc_gL = conduction parameter
ρ	density (kg/m^3)
τ	dimensionless time

Subscripts

g	gas
s	solid

ACKNOWLEDGEMENT

This work was funded by the NASA Lewis Research Center, Stirling Technology Branch, under Contract No. NAS3-26249 (Phase II SBIR). The assistance of N.T. Prokey and J. H. Müller is gratefully acknowledged.

REFERENCES

[1] Pucci, P.F., C.P. Howard and C.H. Piersall, Jr., "The Single-Blow Transient Testing Technique for Compact Heat Exchanger Surfaces," J. Engineering for Power, Vol. 89, January, 1967, pp. 29-40.

[2] Kays, W.M., and London, A.L., *Compact Heat Exchangers*, 3rd ed., McGraw-Hill, 1984.

[3] Walker, G. and V. Vashista, "Heat-Transfer and Flow-Friction Characteristics of Dense-Mesh Wire-Screen Stirling-Cycle Regenerators," Advances in Cryogenic Engineering 16 (1971), pp. 324-332.

[4] Arp, V.D. and R.D. McCarty, "Thermophysical Properties of Helium-4 from 0.8 to 1500 K with Pressures to 2000 MPa," NIST Technical Note 1334, US GPO, 1989.

[5] Bird, R.B., W.E. Stewart and E.N. Lightfoot, *Transport Phenomena*, Wiley, 1960.

[6] Schumann, T.E.W., "Heat Transfer: A Liquid Flowing through a Porous Prism," J. Franklin Inst., 1929, pp. 405-416.

[7] Creswick, F.A., "A Digital Computer Solution of the Equations for Transient Heating of a Porous Solid, Including the Effects of Longitudinal Conduction," *Ind. Math.*, Vol. 8, 1957, pp. 61-68.

[8] Radebaugh, R., and Louie, B. "A Simple, First Step to the Optimization of Regenerator Geometry," In: *Proc. Third Cryocooler Conference*, NBS Special Pub. 698, 1984.

[9] Koester, G., et al, "Oscillating Flow Loss Test Results in Stirling Engine Heat Exchangers", NASA Contractor Report 182288, May, 1990.

REPORT DOCUMENTATION PAGE

Form Approved
OMB No. 0704-0188

1. AGENCY USE ONLY (*Leave blank*)	2. REPORT DATE	3. REPORT TYPE AND DATES COVERED
	January 1997	Final Contractor Report

4. TITLE AND SUBTITLE

Composite Matrix Regenerator for Stirling Engines

5. FUNDING NUMBERS

WU-324-02-00
C-NAS3-26249 SBIR

6. AUTHOR(S)

Timothy R. Knowles

7. PERFORMING ORGANIZATION NAME(S) AND ADDRESS(ES)

Energy Science Laboratories, Inc.
6888 Nancy Ridge Drive
San Diego, California 92121

8. PERFORMING ORGANIZATION REPORT NUMBER

E-10646

9. SPONSORING/MONITORING AGENCY NAME(S) AND ADDRESS(ES)

National Aeronautics and Space Administration
Lewis Research Center
Cleveland, Ohio 44135-3191

10. SPONSORING/MONITORING AGENCY REPORT NUMBER

NASA CR-202322

11. SUPPLEMENTARY NOTES

Project Manager, Diane M. Chapman, Research & Technology Directorate, NASA Lewis Research Center, organization code 5000, (216) 433-2309.

12a. DISTRIBUTION/AVAILABILITY STATEMENT

Unclassified - Unlimited
Released as Publicly Available January 1997.
Subject Categories 20 and 24

This publication is available from the NASA Center for AeroSpace Information, (301) 621-0390.

12b. DISTRIBUTION CODE

13. ABSTRACT (*Maximum 200 words*)

This project concerns the design, fabrication and testing of carbon regenerators for use in Stirling power convertors. Radial fiber design with nonmetallic components offers a number of potential advantages over conventional steel regenerators: reduced conduction and pressure drop losses, and the capability for higher temperature, higher frequency operation. Diverse composite fabrication methods are explored and lessons learned are summarized. A pulsed single-blow test rig has been developed that has been used for generating thermal effectiveness data for different flow velocities. Carbon regenerators have been fabricated by carbon vapor infiltration of electroflocked preforms. Performance data in a small Stirling engine are obtained. Prototype regenerators designed for the HP-1000 power convertor were fabricated and delivered to NASA-Lewis.

14. SUBJECT TERMS

Regenerator; Stirling engines; Carbon; Composite materials; Fabrication; Performance tests; Electroflocking

15. NUMBER OF PAGES

75

16. PRICE CODE

A04

17. SECURITY CLASSIFICATION OF REPORT	18. SECURITY CLASSIFICATION OF THIS PAGE	19. SECURITY CLASSIFICATION OF ABSTRACT	20. LIMITATION OF ABSTRACT
Unclassified	Unclassified	Unclassified	